PHYSICAL REVIEW D **89,** 046008 (2014)

Schrödinger Fermi liquids

Juven Wang[1,2]

[1]*Department of Physics and Center for Theoretical Physics, Massachusetts Institute of Technology, Cambridge, Massachusetts 02139, USA*

[2]*Perimeter Institute for Theoretical Physics, Waterloo, Ontario, Canada N2L 2Y5*

(Received 28 January 2013; published 27 February 2014)

A class of strongly interacting many-body fermionic systems in $2+1$-dimensional nonrelativistic conformal field theory is examined via the gauge-gravity duality correspondence. The five-dimensional charged black hole with asymptotic Schrödinger isometry in the bulk gravity side introduces parameters of background density and finite particle number into the boundary field theory. We propose the holographic dictionary, and realize a quantum phase transition of this fermionic liquid with fixed particle number by tuning the background density β at zero temperature. On the larger β side, we find the signal of a sharp quasiparticle pole on the spectral function $A(k,\omega)$, indicating a well-defined Fermi surface. On the smaller β side, we find only a hump with no sharp peak for $A(k,\omega)$, indicating the disappearance of the Fermi surface. The dynamical exponent z of quasiparticle dispersion goes from being Fermi-liquid-like $z\simeq 1$ scaling at larger β to a non-Fermi-liquid scaling $z\simeq 3/2$ at smaller β. By comparing the structure of Green's function with Landau Fermi liquid theory and Senthil's scaling ansatz, we further investigate the behavior of this quantum phase transition.

DOI: 10.1103/PhysRevD.89.046008 PACS numbers: 11.25.Tq, 04.50.Gh, 71.10.Hf, 05.30.Rt

I. INTRODUCTION

Experimental physics on strongly interacting nonrelativistic many-body bosonic and fermionic systems develops rapidly on account of the progress of controlling ultracold atoms [1–3]. The dynamical exponent z of those microscopic states is usually $z\neq 1$, along with other well-known condensed matter systems such as non-Fermi liquid metals from heavy fermions and high T_c superconductor (see [4,5] and reference therein), beyond the paradigm of Landau Fermi liquid theory. In this strongly coupling regime, the traditional perturbative field theory study has been challenged, while holography, specifically anti–de Sitter space and conformal field theory (AdS/CFT) correspondence [6–8], becomes a powerful alternative. Holographic methods have shown some success in the study of certain strongly interacting fermion systems [9–12], with the emergence of Fermi surface and non-Fermi liquid behavior. (See [13–15] for reviews on the holography applied to condensed matter physics.) However, there are at least two major shortcomings to bridge this success to ultracold atomic systems. On one hand, the dual field theories of this study are asymptotic conformal and relativistic, which are quite different from the nonrelativistic nature of ultracold atoms. On the other hand, this AdS/CFT setting bears no parameters identifying the particle number, mass or density spectrum, because these parameters are not good quantum numbers in the relativistic theory. Tuning physical parameters such as particle number or doping density becomes important in the absolute zero temperature, where purely quantum fluctuations can drive phase transitions, known as quantum phase transitions [16].

Substantial works in the literature had contributed to understand nonrelativistic conformal field theory (NRCFT) ([17–19] and references therein), as a renormalization group fixed point of the nonrelativistic systems. Its gravity dual theory had been proposed, with solutions of zero temperature pure Schrödinger (Schr) geometry [20,21], finite temperature black holes [22–24], and charged black holes [25,26]. There has been some pursuits on studying fermions in this asymptotic Schrödinger geometry [27–29]. However, to our knowledge, the holographic study of the Fermi surface from strongly interacting fermions with NRCFT background has not yet been explored in the literature. Our paper is aimed to bridge this gap and tackle the two aforementioned shortcomings.

The Schrödinger black hole in the bulk gravity theory, on one hand, realizes an asymptotic NRCFT background with the dynamical exponent $z=2$ for the boundary field theory naturally. On the other hand, the Schrödinger black hole provides the particle number (or the mass operator [30]) M from the gauge invariant ξ momentum: $M=\ell-qA_\xi|_{q\partial}$ [30] and background density β to the nonrelativistic boundary field theory. Our approach is similar to the AdS/CFT setup [10], considering a Dirac fermion field in the probe limit under a charged black hole spacetime, the Green's function can be read from the asymptotic behavior of Dirac fermion field in the UV of the bulk side. Here we also propose the holographic dictionary of a real-time retarded Green's function for fermions in Schr/NRCFT correspondence

TABLE I. Conformal dimensions of CFT and NRCFT for spin-0 boson and spin-1/2 fermion.

Asymptotics	AdS_{d+2}	$Schr_{d+3}$
Scalar conformal dimension	$\Delta_\pm = \frac{d+1}{2} \pm \sqrt{(\frac{d+1}{2})^2 + m^2}$	$\Delta_\pm = \frac{d+2}{2} \pm \sqrt{(\frac{d+2}{2})^2 + m^2 + M^2}$
Spinor conformal dimension	$\Delta_\pm = \frac{d+1}{2} \pm m$	$\Delta_\pm = \frac{d+2}{2} \pm \sqrt{(m \pm \frac{1}{2})^2 + M^2}$

[31], analog to the work of [32] for the AdS/CFT case. For convenience, we name these classes of strongly interacting nonrelativistic fermionic liquids under asymptotic NRCFT background as Schrödinger Fermi liquids.

The paper is organized as follows. First, we discuss the charged Schrödinger black hole solution and its Dirac fermion equation of motion, to introduce our notations in Sec. II. We then provide our holographic dictionary [31] analog to the setting of [10,32] in Sec. III. In Sec. IV, we demonstrate the zero temperature nearly ground state of this fermion system shows a sharp quasiparticle peak in the spectral function—the evidence of Fermi surface, with a non-Fermi liquid dispersion relation. We compare our spectral functions $A(k,\omega)$ of Schrödinger Fermi liquids with Landau Fermi liquid theory and Senthil's scaling ansatz 33,34]]. In Sec. V, we show the evidence of a quantum phase transition, by tuning the background density β but fixing the particle number at zero temperature. On the larger β side, we find a well-defined Fermi surface. On the smaller β side, we find only a hump with no sharp peak for $A(k,\omega)$, indicating the disappearance of Fermi surface. The dynamical exponent z of the quasiparticle dispersion goes from Fermi-liquid-like scaling $z=1$ at larger β to larger $z(\simeq 3/2)$ non-Fermi liquid at smaller β. Finally, we conclude with some remarks and open questions in Sec. VI.

Our program code for numerical computation is shared through Supplemental Material [35].

II. SETUP: DIRAC FERMION FIELD IN A CHARGED SCHRöDINGER BLACK HOLE

Based on the holography, a quantum field theory of finite charge density can be mapped to a charged black hole of a gravity theory [10]. The U(1) charge of the Schrödinger black hole induces finite charge density to the boundary field theory, which meanwhile breaks the nonrelativistic conformal invariance. Thus, we only have "asymptotic" NRCFT. Before we discuss the details of bulk gravity theory, it will be helpful to introduce generic labels for a large class of NRCFT (with charge and mass densities) we will study. We characterize our asymptotic NRCFT by five parameters, $(\Delta, M, \mu_Q, \beta, T)$ [30]. Two parameters, the conformal dimension Δ and the mass operator $M = \mathscr{E} - qA_\xi|_\partial$ from the gauge invariant ξ momentum, define the boundary NRCFT in a universal sector. The U(1) charge chemical potential μ_Q and other relevant terms from the current J_μ (such as charge density ρ_Q and mass density ρ_M) in NRCFT is mapped to the U(1) gauge field A_μ of the bulk gravity. Background density β is introduced by the Schrödinger black hole through Null Melvin Twist (or TsT transformation) [22–26]. The physical way to interpret this β could be the density of doping background, or an analog of interaction strength t/U of the Hubbard model.[1] Temperature T of the boundary theory is given by the black hole temperature $T_{\rm BH}$. Notably, the conformal dimension of NRCFT here depends on the mass operator M, which is quite different from CFT. More peculiarly, the conformal dimension for spinors has an extra $m \pm \frac{1}{2}$ split, as already noticed in [27,28]. In the following we denote dimension d as the spatial dimension of $x_1, x_2, \ldots, x_d$. The asymptotic Schrödinger bulk spacetime is denoted as $Schr_{d+3}$ (distinguished from the AdS_{d+2}), where as the corresponding boundary theory of $Schr_{d+3}$ is $NRCFT_{d+1}$ (CFT_{d+1} for AdS_{d+2}). We summarize the conformal dimensions of the spin-0 boson [30] and spin-1/2 fermion operator ([27,28]) in Table I.

A. Charged Schrödinger black hole

We focus on $d=2$, five-dimensional (5D) Schrödinger black hole $Schr_5$ in the bulk and $2+1$D $NRCFT_3$ on the boundary. Let us briefly go through our setup for the charged $Schr_5$. In string frame, the metric is

$$ds^2_{\rm Str} = \frac{Kr^2}{R^2}(-f d\tau^2 + dy^2 - \beta^2 r^2 f(d\tau + dy)^2) + \frac{r^2}{R^2}(dx_1^2 + dx_2^2) + \frac{R^2}{r^2}\frac{dr^2}{f}, \tag{2.1}$$

where R is curvature radius. By converting to light-cone-like coordinates, $t = \beta(\tau + y)$, $\xi = \frac{1}{2\beta}(-\tau + y)$, and switching to the Einstein frame for the later use of holographic dictionary,

$$ds^2_{\rm Ein} = K^{-1/3}\left(\frac{Kr^2}{R^2}\left(\left(\frac{1-f}{4\beta^2} - r^2 f\right)dt^2 + \beta^2(1-f)d\xi^2 + (1+f)dtd\xi\right) + \frac{r^2}{R^2}(dx_1^2 + dx_2^2) + \frac{R^2}{r^2}\frac{dr^2}{f}\right),$$

where $f(r) = 1 + \frac{Q^2}{r^6} - (r_0^4 + \frac{Q^2}{r_0^2})\frac{1}{r^4}$, $K(r) = \frac{1}{1+\beta^2 r^2(1-f(r))}$. The charged black hole supports a gauge field,

[1] Indeed β has dimension [length]^1, so the "background density over area" with correct dimension should be defined as β^{-2}. We simply name β as background density for convenience.

$$A = A_\tau \mathbf{d}\tau, \qquad A_\tau = \frac{Q}{R^2 r_0^2}\left(1 - \frac{r_0^2}{r^2}\right). \tag{2.2}$$

Adopted in [30] notation for later use, $A = \frac{A_\tau}{2\beta} dt - \beta A_\tau d\xi = A_t dt + A_\xi d\xi$, with

$$A_t = \mu_Q + \rho_Q r^{-2}, \qquad A_\xi = M_o + \rho_M r^{-2}. \tag{2.3}$$

By holography [30], μ_Q is identified as U(1) charge chemical potential, ρ_Q, ρ_M are the charge density and mass density, M_o is related to the mass operator by $M = \ell - qA_\xi|_\partial = \ell - qM_o$ with ℓ as the ξ momentum. The temperature of the black hole is given by identifying the inverse of the near-horizon Euclidean periodicity of boundary time coordinate t,

$$T_{\rm BH} = \frac{r_0}{\pi\beta R^2}\left(1 - \frac{Q^2}{2r_0^6}\right). \tag{2.4}$$

Our interest of study is the boundary field theory at zero temperature, which corresponds to the extremal black hole with $Q = \sqrt{2} r_0^3$. This being said, all the numerical analysis contained in this paper pertains to zero temperature only. At zero temperature, the charged black hole Schr_5 horizons degenerate, meanwhile the near horizon geometry becomes $\mathrm{AdSAdS}_2 \times \mathbb{R}^3$, with[2] $ds^2 = -\epsilon^2 d\tilde{\tau}^2/R_{\mathrm{AdS}_2}^2 + R_{\mathrm{AdS}_2}^2 (d\epsilon^2/\epsilon^2) + r_0^2 d\vec{\tilde{x}}^2/R_{\mathrm{AdS}\ 2}^2$, with $R_{\mathrm{AdS}_2} = \frac{(1+\beta^2 r_0^2)^{1/6}}{\sqrt{12}} R$.

B. Dirac fermion

To probe the fermionic response of the boundary theory via holography, we proceed to solve the Dirac fermion equation in the bulk curved spacetime of the charged Schrödinger black hole. The action is

$$S_{\rm Dirac} = \int d^5x \sqrt{-g_{Ein}} i\bar{\psi}(e^\mu_{\hat{a}} \Gamma^{\hat{a}} \mathcal{D}_\mu - m)\psi, \tag{2.5}$$

and its equation of motion (EOM) is $(e^\mu_{\hat{a}} \Gamma^{\hat{a}} \mathcal{D}_\mu - m)\psi = 0$, with covariant derivative

$$\mathcal{D}_\mu = \partial_\mu + \frac{1}{8}\eta_{\hat{a}\hat{c}} \omega^{\hat{c}}_{\hat{b}\mu} [\Gamma^{\hat{a}}, \Gamma^{\hat{b}}] - iqA_\mu, \tag{2.6}$$

where the gamma matrix of flat tangent space $\{\Gamma^{\hat{a}}, \Gamma^{\hat{b}}\} = 2\eta^{\hat{a}\hat{b}}$, vielbeins $e^\mu_{\hat{a}}$ relate flat tangent space to curved spacetime, $g_{\mu\nu} e^\mu_{\hat{a}} e^\nu_{\hat{b}} = \eta_{\hat{a}\hat{b}}$. The spin connection is $\omega^{\hat{c}}_{\hat{b}\mu} = e^{\hat{c}}_\nu \partial_\mu e^\nu_{\hat{b}} + \Gamma^\nu_{\sigma\mu} e^{\hat{c}}_\nu e^\sigma_{\hat{b}}$, $\Gamma^\nu_{\sigma\mu}$ are the Christoffel symbols. We choose the specific vielbein,[3]

$$e^t_{\hat{t}} = K^{\frac{1}{6}} \frac{\beta^2(f-1)}{2r^2 f B}, \qquad e^\xi_{\hat{t}} = K^{\frac{1}{6}} \frac{f + 1 + 2\sqrt{f/K}}{4r^2 f B},$$
$$e^t_{\hat{\xi}} = K^{\frac{1}{6}} B, \qquad e^\xi_{\hat{\xi}} = K^{\frac{1}{6}} \frac{B(f + 1 - 2\sqrt{f/K})}{2\beta^2(f-1)}, \tag{2.7}$$

$$e^{x_1}_{\hat{x_1}} = K^{\frac{1}{6}} 1/r, \quad e^{x_2}_{\hat{x_2}} = K^{\frac{1}{6}} 1/r, \quad e^r_{\hat{r}} = K^{\frac{1}{6}} r\sqrt{f}, \tag{2.8}$$

where other unwritten components of $e^\mu_{\hat{a}}$ are zeros. To simplify the Dirac equation calculation, here B is a function of r chosen ensuring the coefficient of $\Gamma^{\hat{t}}\Gamma^{\hat{\xi}}\Gamma^{\hat{r}}$ in the EOM is zero. The boundary behavior of $B(r \to \infty)$ is a constant B_b times $1/r$. We choose B_b to be 1. Asymptotically, $B(r \to \infty) \simeq \frac{1}{r} + \frac{3\beta^2}{2r^3} + \frac{3(4-4\beta^2-3\beta^4)}{16r^5} + \frac{-16+60\beta^2+24\beta^4+27\beta^6}{32r^7} + \frac{9(48-64\beta^2-24\beta^4-48\beta^6-45\beta^8)}{256r^9} + \cdots$. The near-horizon behavior of B is $B_h/(r-1)$, where B_h is a constant. Given $B_b = 1$, we can numerically solve this equation to find B_h. In 5D spacetime, each of $\Gamma^{\hat{a}}$ matrices has 4×4 components, we choose to express them as follows:

$$\Gamma_\tau = \begin{pmatrix} 0 & i\sigma_3 \\ i\sigma_3 & 0 \end{pmatrix}, \quad \Gamma_y = \begin{pmatrix} 0 & -iI \\ iI & 0 \end{pmatrix}$$
$$\Gamma_{x_1} = \begin{pmatrix} 0 & \sigma_2 \\ \sigma_2 & 0 \end{pmatrix}, \quad \Gamma_{x_2} = \begin{pmatrix} 0 & \sigma_1 \\ \sigma_1 & 0 \end{pmatrix}, \quad \Gamma_r = \begin{pmatrix} I & 0 \\ 0 & -I \end{pmatrix},$$

σ_i are Pauli sigma matrices, I is identity matrix. $\Gamma_t = \beta(\Gamma_\tau + \Gamma_y)$, $\Gamma_\xi = (-\Gamma_\tau + \Gamma_y)/(2\beta)$. Rewrite the four-component Dirac spinor field ψ as

$$\psi = \begin{pmatrix} \psi_+ \\ \psi_- \end{pmatrix} e^{-i\omega t + i\ell\xi + ik_1 x_1 + ik_2 x_2}$$
$$= (-gg^{rr})^{-1/4} \begin{pmatrix} \phi_+ \\ \phi_- \end{pmatrix} e^{-i\omega t + i\ell\xi + ik_1 x_1 + ik_2 x_2}, \tag{2.9}$$

where ϕ_+ and ϕ_- are two-component spinors. This $(-gg^{rr})^{-1/4}$ factor eliminates a Γ_r term in the Dirac equation, which is simplified to

$$(r\sqrt{f}\partial_r \mp mK^{-1/6})\phi_\pm$$
$$\pm \left(\pm u + v\sigma_3 + i\frac{k_1}{r}\sigma_2 + i\frac{k_2}{r}\sigma_1\right)\phi_\mp = 0, \tag{2.10}$$

where u and v are linear combinations of the vielbein components $e^t_{\hat{t}}, e^\xi_{\hat{t}}$, $e^t_{\hat{\xi}}$, and $e^\xi_{\hat{\xi}}$:

$$u = K^{-\frac{1}{6}}\left((\omega + qA_t)\left(-\beta e^t_{\hat{t}} - \frac{1}{2\beta} e^t_{\hat{\xi}}\right)\right.$$
$$\left. + (\ell - qA_\xi)\left(\beta e^\xi_{\hat{t}} + \frac{1}{2\beta} e^\xi_{\hat{\xi}}\right)\right), \tag{2.11}$$

[2] See Appendix A for details.

[3] For convenience, we rescale the coordinates to set $R = r_0 = 1$ from now on.

$$v = K^{-\frac{1}{6}}\left((\omega + qA_t)\left(\beta e^t_{\hat{t}} - \frac{1}{2\beta}e^t_{\hat{\xi}}\right) + (\ell - qA_\xi)\left(-\beta e^\xi_{\hat{t}} + \frac{1}{2\beta}e^\xi_{\hat{\xi}}\right)\right). \quad (2.12)$$

By rotational symmetry of the boundary theory, we will work on the case $k_1 = 0$ and set $k_2 = k$ from here on. We will write $\phi = (\phi_+, \phi_-)^{\mathrm{T}}$, also its $\phi_+ = (y_+, z_+)^{\mathrm{T}}$ and $\phi_- = (y_-, z_-)^{\mathrm{T}}$ in the component form.

III. GREEN'S FUNCTION FROM HOLOGRAPHY

A. Holographic dictionary

We study the fermionic response of the boundary theory, by probing the Dirac fermion field in the bulk spacetime of the Schrödinger black hole. The holographic dictionary of source-response relation can be set up by reading the boundary action of Eq. (2.5). From [32,36], the variation of bulk action induces a boundary term $S_\partial = \int_{\partial\mathcal{M}} d^3x d\xi \sqrt{-g g^{rr}}\bar{\psi}\psi$. Therefore the relation between bulk field and its conjugate momentum are

$$\Pi_+ = -\sqrt{-gg^{rr}}\bar{\psi}_-, \qquad \Pi_- = \sqrt{-gg^{rr}}\bar{\psi}_+. \quad (3.1)$$

We can identify the source (χ) and response ($\mathcal{O}$) from boundary (or UV) behavior of bulk field ($\psi_\pm$) and momentum ($\Pi_\pm$), from the holographic dictionary,

$$\exp[-S_{\mathrm{grav}}[\psi,\bar{\psi}](r\to\infty)] = \left\langle \exp\left[\int d^{d+1}x(\bar{\chi}\mathcal{O} + \bar{\mathcal{O}}\chi)\right]\right\rangle_{\mathrm{QFT}}. \quad (3.2)$$

The source χ and bulk field ψ are related by

$$\chi = \lim_{r\to\infty} r^{\frac{d+1}{2}-\nu_\pm}\psi, \quad (3.3)$$

the response $\mathcal{O}$ and momentum $\Pi_\pm$ are related by

$$\mathcal{O} = -\lim_{r\to\infty} r^{\nu_\pm - \frac{d+1}{2}}\bar{\Pi}, \quad (3.4)$$

where $\nu_\pm = \sqrt{(m\pm\frac{1}{2})^2 + (\ell - qM_o)^2}$ generically,[4] analogue to the result of [32]. Here we show only the standard quantization (corresponding to source A and response D of [32]). The alternate quantization (corresponding to source C and response B of [32]) can be done in the same manner.[5] The Green's function G_R is related to the ratio of $\mathcal{O}$ and χ.

We now study the Dirac equation (2.10) in the boundary UV asymptotic limit to extract $\mathcal{O}$ and χ from the coefficients of ψ and Π, or equivalently related to ϕ_+ and ϕ_- at $r\to\infty$. In this limit, (2.10) becomes

$$(r\sqrt{f}\partial_r \mp mK^{-1/6})\phi_\pm + \left(\frac{(\ell+qQ\beta)r}{2\beta}P_\pm + \frac{\mathcal{C}}{r}P_\pm + \frac{2\beta(\ell+qQ\beta)}{r}P_\mp \pm \frac{ik_1}{r}\sigma_2 \pm \frac{ik_2}{r}\sigma_1\right)\phi_\mp = 0,$$

where

$$\mathcal{C} = \frac{1}{8\beta^2}(-4\ \mathrm{qQ}(1+\beta^2) + 5(\ell+qQ\beta)\beta^3 - (\ell+qQ\beta)Q^2\beta^3 - 8\beta\omega),$$
$$P_\pm = \frac{1\pm\sigma_3}{2}$$

$$\phi_+ = \mathbf{S}_1 r^{\nu_+ - \frac{1}{2}}(A_1 + A_2 r^{-2}) + \mathbf{R}_1 r^{-\nu_+ - \frac{1}{2}}(\alpha_1 + \alpha_2 r^{-2}) + \mathbf{S}_2 r^{\nu_- + \frac{1}{2}}(B_1 + B_2 r^{-2}) + \mathbf{R}_2 r^{-\nu_- + \frac{1}{2}}(\beta_1 + \beta_2 r^{-2}) + \cdots, \quad (3.7)$$

$$\phi_- = \mathbf{S}_1 r^{\nu_+ + \frac{1}{2}}(C_1 + C_2 r^{-2}) + \mathbf{R}_1 r^{-\nu_+ + \frac{1}{2}}(\gamma_1 + \gamma_2 r^{-2}) + \mathbf{S}_2 r^{\nu_- - \frac{1}{2}}(D_1 + D_2 r^{-2}) + \mathbf{R}_2 r^{-\nu_- - \frac{1}{2}}(\delta_1 + \delta_2 r^{-2}) + \cdots, \quad (3.8)$$

here

$$\nu_\pm = \sqrt{(m\pm 1/2)^2 + (\ell+qQ\beta)^2}. \quad (3.9)$$

Each of $\mathbf{S}_1, \mathbf{S}_2, \mathbf{R}_1, \mathbf{R}_2$ is an r-independent one-component multiplier, as the coefficient of the spinor.[6] There is a projection relation between the two-component spinors[7]:

[4] Specifically ν equals to $\sqrt{(m\pm 1/2)^2 + (\ell+qQ\beta)^2}$ in our charged Schrödinger black hole case.

[5] For the alternate quantization,

$$\chi = \lim_{r\to\infty} r^{\frac{d+3}{2}-\nu_\pm}\psi, \quad (3.5)$$

the response $\mathcal{O}$ and momentum $\Pi_\pm$ are related by

$$\mathcal{O} = \lim_{r\to\infty} r^{\nu_\pm - \frac{d+3}{2}}\Pi. \quad (3.6)$$

[6] When doing numerics for this field redefinition, it is important to keep subleading term C_2 in the $\mathbf{S}_1 r^{\nu_+ + \frac{1}{2}}(\cdots + C_2 r^{-2} + \cdots)$ series, since this C_2 term dominates $R_1 r^{-\nu_+ - \frac{1}{2}}\alpha_1$ when $\nu_+ > \frac{1}{2}$, which is indeed our case in the numerical study. Thus here we keep the expansion for all four sets of solutions to the subleading orders.

[7] Each of $A_1, A_2, C_1, C_2, \alpha_1, \alpha_2, \gamma_1, \gamma_2, B_1, B_2, D_1, D_2, \beta_1, \beta_2, \delta_1, \delta_2$ is a two-component spinor. List above totally there are sixteen two-component spinors. The spinors C_1, C_2, γ_1, and γ_2 are in the null space of P_+, the spinors B_1, B_2, β_1, and β_2 are in the null space of P_-. There are four independent sets of bases, each basis as a solution of Dirac EOM: the first set contains A_1, A_2, C_1, C_2 and its subleading terms, the second set contains $\alpha_1, \alpha_2, \gamma_1, \gamma_2$ and its subleadings, the third set contains B_1, B_2, D_1, D_2 and its subleadings, the fourth set contains $\beta_1, \beta_2, \delta_1, \delta_2$ and its subleadings.

$$\mathbf{S}_1 C_1 = \frac{-(\ell + qQ\beta)}{2\beta(\nu_+ + m + \frac{1}{2})} P_- \mathbf{S}_1 A_1,$$
$$\mathbf{S}_2 B_1 = \frac{-(\ell + qQ\beta)}{2\beta(\nu_- - m + \frac{1}{2})} P_+ \mathbf{S}_2 D_1, \tag{3.10}$$

$$\mathbf{R}_1 \gamma_1 = \frac{-(\ell + qQ\beta)}{2\beta(-\nu_+ + m + \frac{1}{2})} P_- \mathbf{R}_1 \alpha_1,$$
$$\mathbf{R}_2 \beta_1 = \frac{-(\ell + qQ\beta)}{2\beta(-\nu_- - m + \frac{1}{2})} P_+ \mathbf{R}_2 \delta_1. \tag{3.11}$$

We now apply our holographic dictionary to identify the source and response from (3.7) and (3.8). To read the boundary value, in the following we take $r \to \infty$ as the UV limit. Consider the leading behavior of the ϕ_- contribution,

$$\psi_- = (-gg^{rr})^{-1/4}\phi_- \simeq r^{-2}\phi_- \simeq \mathbf{S}_1 C_1 r^{\nu_+ - 3/2} \tag{3.12}$$

which corresponds to the source χ_-,

$$\chi_- = \lim_{r\to\infty} r^{\frac{3}{2}-\nu_+}\psi_- \simeq \mathbf{S}_1 C_1, \tag{3.13}$$

χ_- is proportional to $\mathbf{S}_1$. The momentum field $\bar{\Pi}_-$ is

$$\bar{\Pi}_- = \sqrt{-gg^{rr}}\psi_+ = (-gg^{rr})^{1/4}\phi_+ \simeq r^2\phi_+ \simeq \mathbf{S}_1 A_1 r^{\nu_+ + 3/2} + \mathbf{R}_1 \alpha_1 r^{-\nu_+ + 3/2} + \cdots \tag{3.14}$$

which corresponds to the response O_-,

$$O_- = \lim_{r\to\infty} r^{\nu_+ - \frac{3}{2}}\bar{\Pi}_- \simeq \mathbf{R}_1 \alpha_1. \tag{3.15}$$

We take the asymptotic constant term on the UV boundary. O_- is proportional to $\mathbf{R}_1$.

On the other hand, we can go through the same logic again, though consider the leading behavior of ϕ_+ contribution,

$$\psi_+ = (-gg^{rr})^{-1/4}\phi_+ \simeq r^{-2}\phi_+ \simeq \mathbf{S}_2 B_1 r^{\nu_- - 3/2} \tag{3.16}$$

which corresponds to the source χ_+,

$$\chi_+ = \lim_{r\to\infty} r^{\frac{3}{2}-\nu_-}\psi_+ \simeq \mathbf{S}_2 B_1, \tag{3.17}$$

χ_+ is proportional to S_2. The momentum field Π_+ is

$$\bar{\Pi}_+ = -\sqrt{-gg^{rr}}\psi_- = -(-gg^{rr})^{1/4}\phi_- \simeq -r^2\phi_- \simeq -\mathbf{S}_2 D_1 r^{\nu_- + 3/2} - \mathbf{R}_2 \delta_1 r^{-\nu_- + 3/2} + \cdots \tag{3.18}$$

which corresponds to the response O_+,

$$O_+ = -\lim_{r\to\infty} r^{\nu_- - \frac{3}{2}}\bar{\Pi}_+ \simeq \mathbf{R}_2 \delta_1, \tag{3.19}$$

O_+ is proportional to $\mathbf{R}_2$. Now we derive $\mathbf{S}_1$, $\mathbf{S}_2$ are identified as sources, $\mathbf{R}_1$, $\mathbf{R}_2$ are identified as responses for this standard quantization. A similar argument works for the alternative quantization by taking the subleading terms of the bulk field and its conjugate momentum; we leave this detail to Appendix C.

In addition to the above dictionary, we provide another intuitive argument on identifying source and response. We notice the boundary action $\bar{\psi}\psi$, due to the Γ_τ form; it couples the first component of the spinor ψ to the third component of ψ, which couples the second component of ψ to the fourth component of ψ. Both two-point function or $\bar{\psi}\psi$ shows $r^{2\nu_+}$ scaling in [27] and [28] and our work. However, the $r^{2\nu_-}$ scaling is only seen in our and the Green's functions of [28]. We will perform a more constructive comparison with [27] and [28] and a pure Schrödinger Green's function computation via our dictionary in Appendix D. Lastly, we are aware that the detailed construction of the Schr/NRCFT holographic dictionary involves nontrivial holographic renormalization [28,37,38]. Our work here only follows the strategy in Refs. [10,32] constructing the source-response holographic dictionary. The rigorous holographic renormalization for spinors is the future step to justify the complete dictionary for the Green's function.

B. Source and response from UV expansion

To extract the data of source and response, we define a converting matrix $\mathrm{C_v}$ as a function of r (see Appendix B and a shared program code through a URL link), and a set of functions $\mathbf{S}_1(r)$, $\mathbf{S}_2(r)$, $\mathbf{R}_1(r)$, $\mathbf{R}_2(r)$ satisfies

$$\varphi(r) = (\varphi_+(r)\varphi_-(r))^{\mathrm{T}} = (y_+(r)z_+(r)y_-(r)z_-(r))^{\mathrm{T}} = \mathrm{C_v}\cdot[\mathbf{S}_1(r)\mathbf{R}_1(r)\mathbf{S}_2(r)\mathbf{R}_2(r)]^{\mathrm{T}}. \tag{3.20}$$

By this field definition, neatly $\mathbf{S}_1(r)$, $\mathbf{S}_2(r)$, $\mathbf{R}_1(r)$, $\mathbf{R}_2(r)$ approach to $\mathbf{S}_1$, $\mathbf{S}_2$, $\mathbf{R}_1$, $\mathbf{R}_2$ as $r \to \infty$. Due to projection, we find the spinors have the properties $c_{1+} = c_{2+} = \gamma_{1+} = \gamma_{2+} = b_{1-} = b_{2-} = \beta_{1-} = \beta_{2-} = 0$. To deal with the standard quantization, from the lesson of Sec. III A, we choose $c_{1-} = 1$ to compute the first set of bases, $\alpha_{1-} = 1$ to compute the second set of bases, $b_{1+} = 1$ to compute the third set of bases, and $\delta_{1+} = 1$ to compute the fourth set of bases. Each of four independent bases in (3.7) and (3.8) (equivalently in (B2), see [7]), can be determined by a free parameter, thus totally four free parameters. Now the four free parameters for four independent bases are $\mathbf{S}_1$, $\mathbf{S}_2$, $\mathbf{R}_1$, $\mathbf{R}_2$. Argue from Sec. III A, for the standard quantization, the source terms are $\mathbf{S}_1 C_1$, $\mathbf{S}_2 B_1$, with their corresponding response terms $\mathbf{R}_1\alpha_1$, $\mathbf{R}_2\delta_1$, respectively. Our choice of spinor $C_1^T = (0,1)$ and its coupled spinor $\alpha_1^T = (\alpha_{1+}, 1)$ justifies that coefficient $\mathbf{S}_1$ is exactly a source and $\mathbf{R}_1$ is its response. Our choice of spinor $B_1^T = (1,0)$ and its coupled spinor $\delta_1^T = (1, \delta_{1-})$

justifies that coefficient $\mathbf{S}_2$ is exactly a source and $\mathbf{R}_2$ is its response.[8]

C. IR behavior and the infalling boundary condition

To determine the near horizon initial condition of the Dirac equation, here we deal with IR behavior and solve the infalling boundary condition at zero temperature, $Q = \sqrt{2}$. Consider the small ϵ expansion of the equations, where $r = 1 + \epsilon$. The equation for $B(r)$ becomes $\frac{B'}{B} = -1/\epsilon$. Thus, we take the behavior of $B(r)$ near horizon as B_h/ϵ, where B_h is another constant, $\lim_{r\to 1}(r-1)B(r) = B_h$. For the later use, we define

$$\tilde{\omega} = \frac{\ell}{2\beta} + \beta\omega, \tag{3.21}$$

$\tilde{\omega}$ is the coefficient of τ in the exponent dependence of Eq. (2.9). We find that the behavior of f, u, v in the IR is given by

$$f \to 12\epsilon^2, \qquad u \to \frac{i\tilde{\omega}}{\epsilon}U, \qquad v \to \frac{i\tilde{\omega}}{\epsilon}V \tag{3.22}$$

with $U \equiv \frac{i}{4\sqrt{3}}\left(\frac{2\sqrt{3}B_h}{\beta^2} - \frac{\beta^2}{2\sqrt{3}B_h}\right)$ and $V \equiv \frac{i}{4\sqrt{3}}\left(\frac{2\sqrt{3}B_h}{\beta^2} + \frac{\beta^2}{2\sqrt{3}B_h}\right)$. The Dirac equation near horizon and its infalling wave function ansatz are

$$\epsilon^2\phi'_{\pm} = \frac{-i}{2\sqrt{3}}\tilde{\omega}(U \pm V\sigma_3)\phi_{\mp} \tag{3.23}$$

$$\phi_{\pm} \propto e^{+i\tilde{\omega}/(12\epsilon)}. \tag{3.24}$$

The exponent of wave function $\phi_{\pm}$ is chosen to be a $+$ sign, in order to combine with Eq. (2.9) to be $e^{-i\tilde{\omega}\tau + i\tilde{\omega}/(12\epsilon)}$ infalling into the black hole.[9] The infalling condition is obtained by plugging Eq. (3.24) into Eq. (3.23), where the subscript H stands for values at the horizon:

$$\phi_+|_H = (U + V\sigma_3)\phi_-|_H. \tag{3.25}$$

The infalling condition for spinors has two linear independent choices, the first set is $\phi_{-,1} = (1, 0)$ thus $\phi_{+,1} = (U + V, 0)$, and the second set is $\phi_{-,2} = (0, 1)$ thus $\phi_{+,2} = (0, U - V)$.

[8]For the alternate quantization, we should alternatively choose $a_{1-} = 1$ to compute the first set of bases, $\gamma_{1-} = 1$ to compute the second set of bases, $d_{1+} = 1$ to compute the third set of bases, $\beta_{1+} = 1$ to compute the fourth set of bases. From Sec. III A, the source terms are $\mathbf{S}_2 D_1$, $\mathbf{S}_1 A_1$; with their corresponding response terms $\mathbf{R}_2\beta_1$, $\mathbf{R}_1\gamma_1$, respectively. Our choice of spinor $A_1^T = (a_{1+}, 1)$ and its coupled spinor $\gamma_1^T = (0, 1)$ justifies that coefficient $\mathbf{S}_1$ is exactly a source and $\mathbf{R}_1$ is its response. Our choice of spinor $D_1^T = (1, d_{1-})$ and its coupled spinor $\beta_1^T = (1, 0)$ justifies that coefficient $\mathbf{S}_2$ is exactly a source and $\mathbf{R}_2$ is its response.

[9]The 12 factor appearing here originates from the near horizon geometry AdS_2.

Therefore this gives two independent sets of initial conditions at horizon for $\mathbf{S}_1(r), \mathbf{R}_1(r), \mathbf{S}_2(r), \mathbf{R}_2(r)$, where we introduce one more upper indices 1, 2 to distinguish the first and the second sets:

$$\begin{aligned}[\mathbf{S}_\mathbf{1}^1(r)\mathbf{R}_\mathbf{1}^1(r)\mathbf{S}_\mathbf{2}^1(r)\mathbf{R}_\mathbf{2}^1(r)]^{\mathrm{T}}|_H &= \mathrm{C_v}^{-1}|_H \cdot (\phi_{+,1}\phi_{-,1})^{\mathrm{T}}|_H \\ &= \mathrm{C_v}^{-1}|_H \cdot (U + V010)^{\mathrm{T}}, \\ [\mathbf{S}_\mathbf{1}^2(r)\mathbf{R}_\mathbf{1}^2(r)\mathbf{S}_\mathbf{2}^2(r)\mathbf{R}_\mathbf{2}^2(r)]^{\mathrm{T}}|_H &= \mathrm{C_v}^{-1}|_H \cdot (\phi_{+,2}\phi_{-,2})^{\mathrm{T}}|_H \\ &= \mathrm{C_v}^{-1}|_H \cdot (0U - V01)^{\mathrm{T}}.\end{aligned}$$

More conveniently in matrix form,

$$\mathbf{S}(r) = \begin{bmatrix} \mathbf{S}_\mathbf{1}^1(r) & \mathbf{S}_\mathbf{1}^2(r) \\ \mathbf{S}_\mathbf{2}^1(r) & \mathbf{S}_\mathbf{2}^2(r) \end{bmatrix}, \qquad \mathbf{R}(r) = \begin{bmatrix} \mathbf{R}_\mathbf{1}^1(r) & \mathbf{R}_\mathbf{1}^2(r) \\ \mathbf{R}_\mathbf{2}^1(r) & \mathbf{R}_\mathbf{2}^2(r) \end{bmatrix},$$

D. Green's function

Green's function of the boundary theory is defined to be the ratio between source matrix $\mathbf{S}(r)$ and response matrix $\mathbf{R}(r)$. Thus we define $\mathbf{G}(r)$ based on $\mathbf{R}(r) = \mathbf{G}(r)\mathbf{S}(r)$, and evaluate $\mathbf{G}(r)$ at $r \to \infty$, to read the 2×2 matrix Green's function $\mathbf{G}$ of the boundary theory,[10]

$$\mathbf{G} = \lim_{r\to\infty}\mathbf{G}(r) = \lim_{r\to\infty}\mathbf{R}(r)\mathbf{S}(r)^{-1}. \tag{3.26}$$

We derive the EOM of $\mathbf{G}(r)$ in the bulk gravity (see Appendix B), and solve this EOM with the initial condition: $\mathbf{G}(r)|_H = \mathbf{R}(r)|_H \cdot \mathbf{S}(r)^{-1}|_H$ to obtain physical results of Eq. 3.26.

IV. SPECTRAL FUNCTION $A(k,\omega)$

We now equip with the holography tool developed in Secs. II and III. The original questions driving our interests are: What is the nearly ground state of this fermionic system under asymptotic NRCFT background at zero temperature? Will there be a Fermi surface? Will Fermi surface collapse, destabilized by tuning non-temperature parameters (such as background density β)? Will this realize a certain quantum phase transition of fermionic liquids? With the holographic dictionary for Green's function, we proceed to study these questions. We focus on $Q = \sqrt{2}$ as zero temperature phase.

The spectral function $A(k, \omega)$ of this boundary system can be determined by the imaginary part of Green's function. In $2 + 1$ D boundary theory with 2×2 matrix

[10]There is no extra Γ^τ factor multiplied with $G(r)$ for this Green's function, because in our dictionary sources and responses are related to the coefficients of two-component spinors, instead of spinors itself.

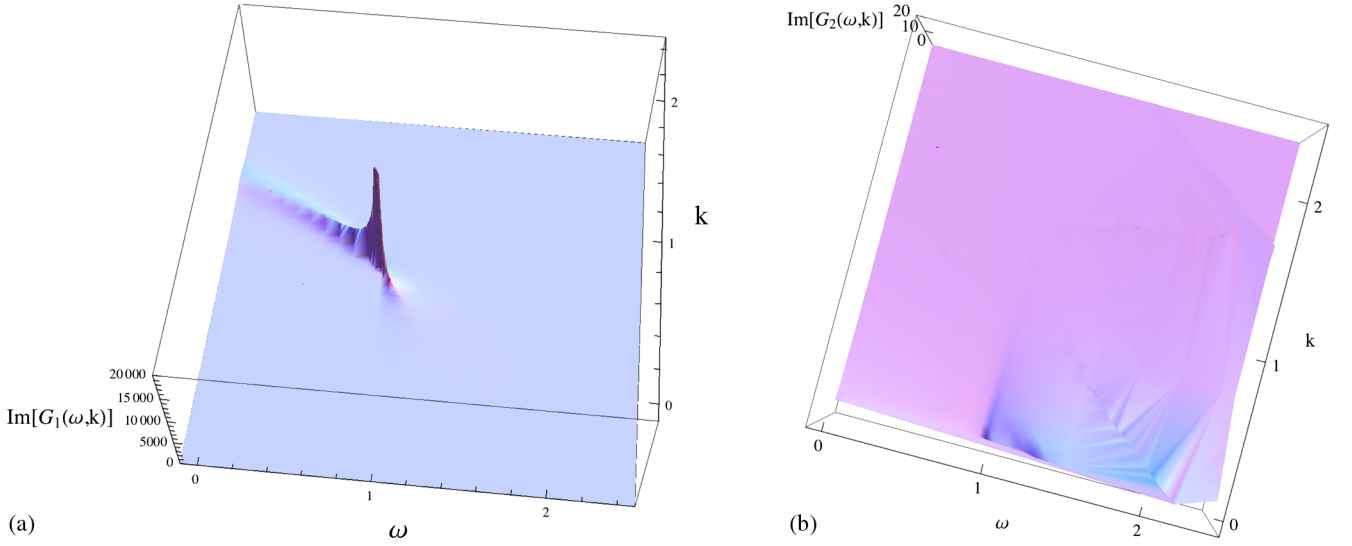

FIG. 1 (color online). At $\beta = 1/\sqrt{2}$, (a) the imaginary part of Green's function, $\mathrm{Im}[G_1]$ as a function of ω and k. A sharp quasiparticle-like pole at $\omega_F = 0.8984$, $k_F = 1.3169$ indicates a well-defined Fermi surface. The pole indicates an infinite lifetime stable quasiparticle at k_F. Notice the main branch of dispersion goes into $\omega < \omega_F$ and $k > k_F$, a holelike excitation. While in [10], their main branches of dispersion goes into $\omega > \omega_F$ and $k > k_F$, a particlelike excitation. (b) The imaginary part of Green's function, $\mathrm{Im}[G_2]$ as a function of ω and k; it is more or less featureless, except a wedgelike structure.

$\mathbf{G}$, we should take eigenvalues of $\mathbf{G}$, namely, $\mathrm{Im}[\mathbf{G}(r \to \infty)_{\mathrm{eigenvalues}}]$.[11]

A. Fermi surface

This nonrelativistic fermionic system has five parameters, conformal dimensions $\Delta_\pm(\nu_\pm)$, temperature T, chemical potential (of background) μ_Q, particle number eigenvalue or mass M, and background density β. We first study the background density at $\beta = 1/\sqrt{2}$ at $T = 0$. The gauge-invariant mass operator $M \equiv \ell - qM_o = \ell + qQ\beta$ is fixed to be $1/10$. The Dirac fermion charge $q = 1$, its mass is chosen to be $m = 1/10$, nonzero value in order to avoid scaling dimension $\nu_\pm$ degeneracy and extra logarithmic term in UV expansion.

Similar to [10], among two eigenvalues (say $\mathbf{G}_1, \mathbf{G}_2$) one of the eigenvalues, $\mathbf{G}_1$ with its imaginary $\mathrm{Im}[\mathbf{G}_1]$ has shown a polelike structure [see Fig. 1], thus is picked for detailed studies in our analysis. The other eigenvalue $\mathbf{G}_2$ with its imaginary $\mathrm{Im}[\mathbf{G}_2]$, only shows less-distinguished wedge-like structure [see Fig. 1], which appears to be less interesting physically. Following [10], we focus on studying one of these eigenvalues, $\mathbf{G}_1$. Below we will simply abbreviate $\mathrm{Im}[\mathbf{G}_1]$, $\mathrm{Re}[\mathbf{G}_1]$ as $\mathrm{Im}G_1$, $\mathrm{Re}G_1$. We find there is a sharp pole on $\mathrm{Im}[G_1]$ at $\omega_F = 0.8984$, $k_F = 1.3169$, indicating a stable quasiparticle like excitation at Fermi-momentum k_F. This indicates a well-defined Fermi surface. Normally the location of Fermi surface on the ω axis is shifted by chemical potential μ, one redefines $\bar{\omega} = \omega - \mu$ thus $\bar{\omega} = 0$ has the Fermi surface. In our case, ω_F is shifted by the presence of ξ momentum ℓ, this can be realized from the fact that the location of Fermi surface is determined mainly from the low energy IR physics. which in the bulk gravity corresponds to the near horizon region. Thus, instead of using boundary time coordinate t and its coupled conjugate energy ω, we identify the near-horizon time coordinate τ and its conjugate energy $\tilde{\omega}$. When $\tilde{\omega} = (\frac{\ell}{2\beta} + \beta\omega)|_{\omega_F} = 0$, namely $\omega_F = -\ell/(2\beta^2)$, its value indicates the pole location of a Fermi surface. Denote $k_\perp \equiv |k - k_F|$, we find near the quasiparticle like peak has scalings,

$$\omega_*(k_\perp) \sim k_\perp^z, \qquad z \simeq 1.14 \tag{4.2}$$

$$\mathrm{Im}[G_1(\omega_*(k_\perp), k_\perp)] \sim k_\perp^{-\alpha}, \qquad \alpha \simeq 1.00. \tag{4.3}$$

[11] In principle, the spectral function is written as

$$A(k,\omega) = -\frac{1}{\pi}\mathrm{Im}[G]. \tag{4.1}$$

The usual angle resolved photoemission spectroscopy (ARPES) data [39] sum rule is $\int_{-\infty}^{\infty} A(k,\omega)d\omega = 1$ [39]. This ARPES sum rule holds in a nonrelativistic system. The relativistic version of sum rule is written as, see Ref. [40], $\int_{-\infty}^{\infty} \omega A(k,\omega)d\omega = 1$. In the context of gauge-gravity duality, the modification of the ARPES sum rule has been studied [41], e.g. see a comment at Eq. (5.27) of Ref. [41]. To produce any of the above sum rules, we comment on a subtlety in Schrödinger holography. When we relate the $d+3$-D gravity theory to a $d+1$-D boundary theory via Eq. (3.2), the constant factor $\int d\xi \equiv L_\xi$ needs to be absorbed into $\int d^{d+1}x(\bar{\chi}\mathcal{O} + \bar{\mathcal{O}}\chi)$; this gives an extra constant factor for source field or response field. Namely, the $A(k,\omega)$ may be different from $\mathrm{Im}[\mathbf{G}]$ with another extra constant factor. This factor should be important when justifying the spectral density sum rule, $\int_{-\infty}^{\infty} A(k,\omega)d\omega = 1$. The exact value of our $\mathrm{Im}[\mathbf{G}]$ is less informative, only the relative height of $\mathrm{Im}[\mathbf{G}]$ has physical indication. In addition, we are aware that there is an alternative proposal to study the trace part [11], $\mathrm{Im}[\mathrm{Tr}[\mathbf{G}(r \to \infty)]]$.

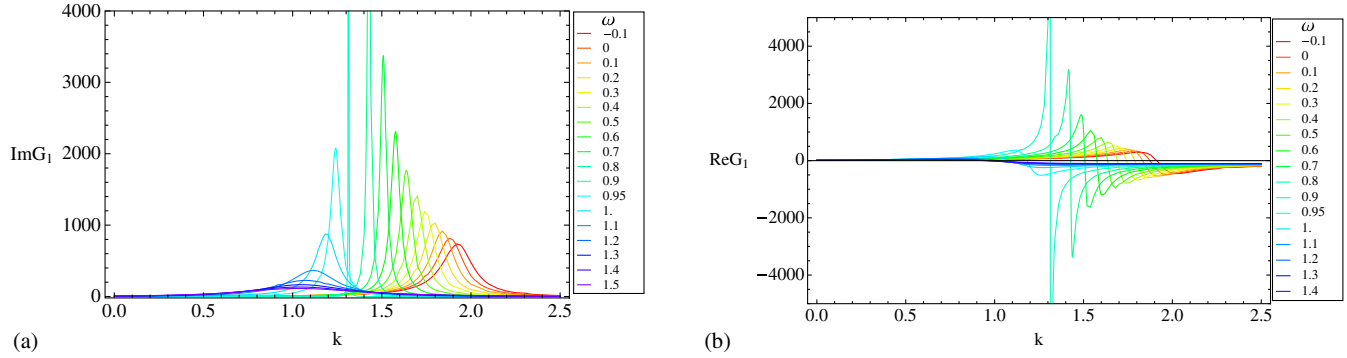

FIG. 2 (color online). At $\beta = 1\sqrt{2}$, (a) the imaginary part of Green's function, with a pole. (b) The real part of Green's function switches sign crossing zero value at a specific ω near the peak of $\mathrm{Im}[G_1]$.

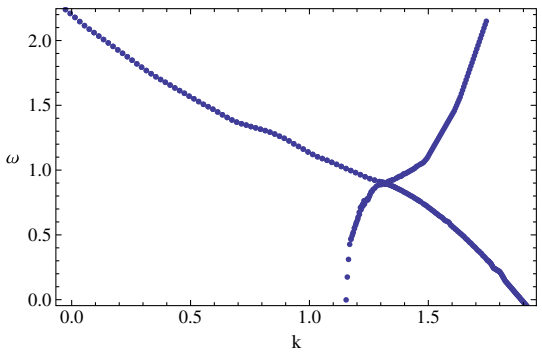

FIG. 3 (color online). The dispersion relation traces the pole into four branches on the (k, ω) plane in a large scale. The asymmetric behavior indicates a particle-hole asymmetry.

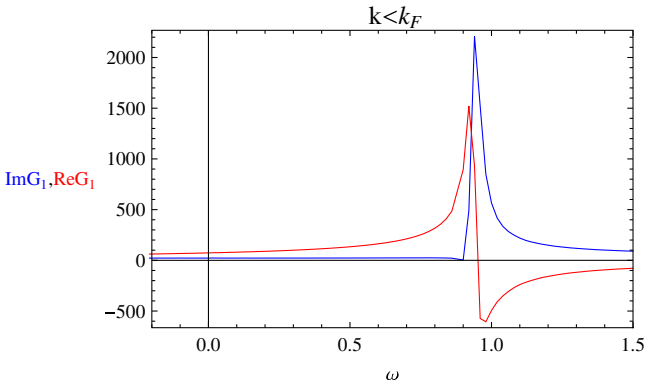

FIG. 4 (color online). $k = 621/500 < k_F$. The blue curve is for $\mathrm{Im}\, G_1$; the red curve is for $\mathrm{Re}\, G_1$.

In Fig. 2, we show the imaginary part $\mathrm{Im}[\mathbf{G}_1]$ and real part $\mathrm{Re}[\mathbf{G}_1]$ of Green's function; see the location of the Fermi surface indicates a pole in $\mathrm{Im}[\mathbf{G}_1]$ and switches the sign of $\mathrm{Re}[\mathbf{G}_1]$. The main branch of dispersion goes into $\omega < \omega_F$ and $k > k_F$, which is a holelike excitation. The result is different from [10], where their main branches go into a particlelike excitation with $\omega > \omega_F$ and $k > k_F$. In Fig. 3, the dispersion relation shows particle-hole asymmetry in large scale, though close to (ω_F, k_F) it gives a unique dynamical exponent z.

B. Comparison to Landau Fermi liquid theory and Senthil's scaling ansatz

To better understand the physics of Green's function $G(k, \omega)$, we now study the functional form of $G(k, \omega)$ in terms of two different classes. Both classes hold under general arguments. The first class is Landau Fermi liquid theory, which holds for the weak coupling system, where the free fixed point is still a good description of the system. The second class is even more general based on scaling ansatz for non-Fermi liquid theory and critical Fermi surface, proposed by Senthil [33,34]. In Landau Fermi liquid (LFL) theory, the retarded Green's function is of the form

$$\begin{aligned} G(k,\omega) &= \frac{1}{\omega - \xi_k - \Sigma(\omega,k)} \\ &= \frac{1}{\omega - (\xi_k + \mathrm{Re}\Sigma(k,\omega)) - i\mathrm{Im}\Sigma(k,\omega)} \\ &= \frac{Z}{(\omega-\omega_F) - \tilde{\xi}_k + \frac{i}{2\tilde{\tau}_k}}. \end{aligned} \tag{4.4}$$

$\Sigma(\omega, k)$ is the particle irreducible retarded self-energy. $\xi_k \equiv \varepsilon_k - \mu$ is the excitation around the original chemical potential. The condition $\xi_{k_F} + \mathrm{Re}\Sigma(k_F, \omega_F) = \omega_F$ to define renormalized Fermi-momentum k_F. The final form is obtained by expanding $\xi_k + \mathrm{Re}\Sigma(k, \omega)$ around (k_F, ω_F), with the definition of quasiparticle residue Z, with $Z^{-1} \equiv 1 - \frac{\partial}{\partial\omega}\mathrm{Re}\Sigma(k = k_F, \omega = \omega_F)$, also $\tilde{\xi}_k \equiv (k - k_F) Z \frac{\partial}{\partial k}(\xi_{k_F} + \mathrm{Re}\Sigma(k_F, \omega_F)) \equiv v(k - k_F)$, and quasiparticle decay rate $1/\tau_k \equiv -2Z\,\mathrm{Im}\,\Sigma(k, \omega)$. The specific LFL form we use to fit our Green's function is

$$G = \frac{Z}{(-(\omega - \omega_F) - v(k - k_F)) - i\gamma(\omega)} \tag{4.5}$$

with our quasiparticle self-energy ansatz as $\gamma(\omega) = \kappa(\omega - \omega_F)^n$, where κ is some real constant, LFL has

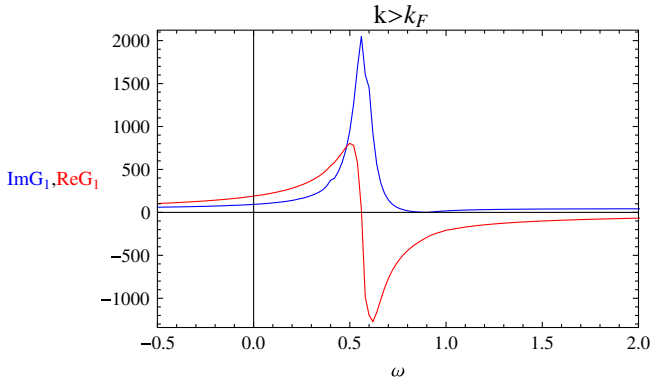

FIG. 5 (color online). $k = 8/5 > k_F$. The blue curve is for $\mathrm{Im}\, G_1$; the red curve is for $\mathrm{Re}\, G_1$.

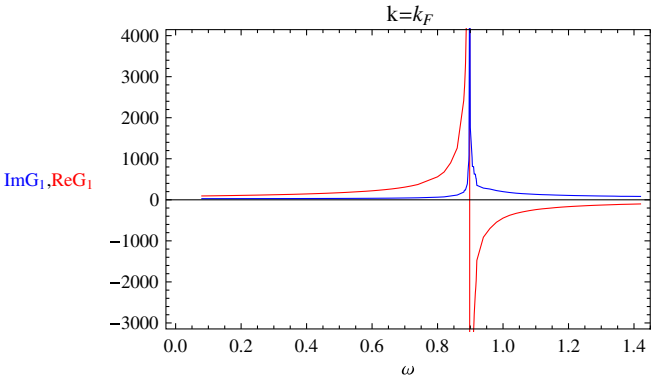

FIG. 6 (color online). $k = k_F$. The blue curve is for $\mathrm{Im}\, G_1$ the red curve is for $\mathrm{Re}\, G_1$.

$n = 2$. We will take general n for fitting ansatz. We flip the sign of $(\omega - \omega_F)$ to have a holelike dominant excitation as Fig. 3 suggests.

The scaling ansatz proposed by Senthil [33,34] based on general arguments, has the form at $T = 0$,

$$G = c_0(k - k_F)^{-\alpha} F_0\left(\frac{c_1(\omega - \omega_F)}{(k - k_F)^z}\right). \tag{4.6}$$

In order to have the best fitting, we will be forced to choose c_0 and c_1 their values on two sides $\omega > \omega_F$ and $\omega < \omega_F$ differently to reflect particle-hole asymmetry.

In the following subsections, we present our Green's function data for $k < k_F$, $k = k_F$, and $k \simeq k_F$, and fit these data by LFL and Senthil's ansatz. The main message of fitting our data (Figs. 4, 5, and 6) to LFL and Senthil's ansatz (Figs. 7, 8, and 9) are:

(1) Senthil's ansatz generally has better agreement than LFL fitting for our ImG_1 data.

(2) Our ReG data are sandwiched by the LFL fitting with LFL fitting with $n = 2$ and marginal Fermi liquid (MFL) with $n = 1$ [42,43], which likely implies that our Schrödinger Fermi liquids can be a closer description between LFL and MFL theory with $1 < n < 2$. From our quasiparticle self-energy ansatz as $\gamma(\omega) = \kappa(\omega - \omega_F)^n$ and quasiparticle decay rate $1/\tau_k \sim \gamma(\omega)$, this may suggest Schrödinger Fermi liquids have shorter lifetime

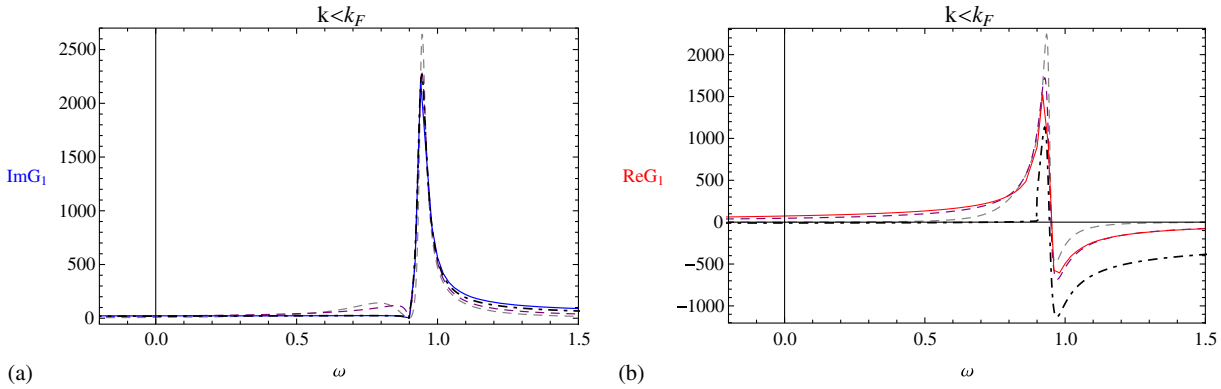

FIG. 7 (color online). $k = 621/500 < k_F$, both (a) and (b) with three fitting curves: (1) LFL Eq. (4.5) with $n = 2$ in the gray-dashed line, (2) LFL Eq. (4.5) with $n = 1$ in the purple-dashed line, (3) scaling ansatz form Eq. (4.8) in the black-dot-dashed line. c_0, c_1, γ_0 are chosen to be positive but their values on two sides $\omega > \omega_F$ and $\omega < \omega_F$ are chosen differently.

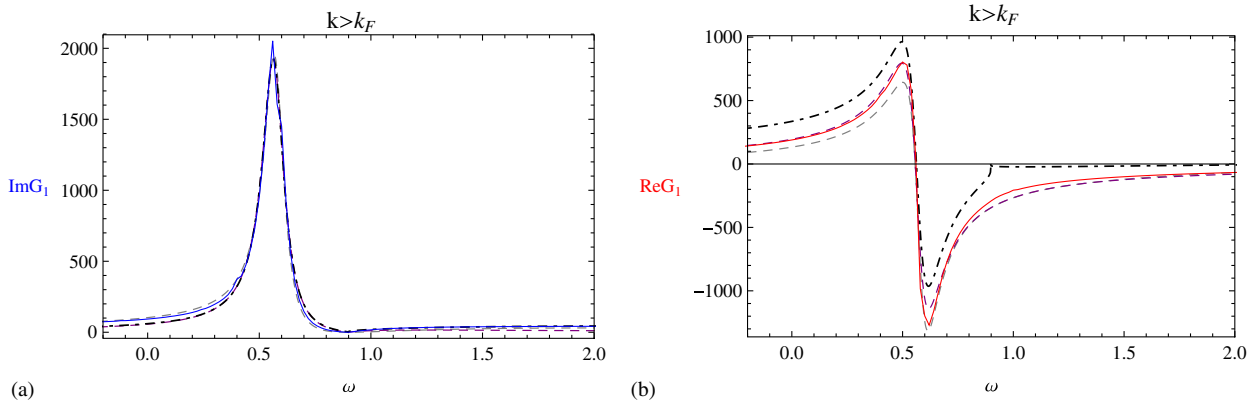

FIG. 8 (color online). $k = 8/5 > k_F$, both (a) and (b) with three fitting curves: (1) LFL Eq. (4.5) with $n = 2$ in the gray-dashed line, (2) LFL Eq. (4.5) with $n = 1$ in the purple-dashed line, and (3) scaling ansatz form Eq. (4.10) in the black-dot-dashed line. c_0, c_1, γ_0 are chosen to be positive but their values on two sides $\omega > \omega_F$ and $\omega < \omega_F$ are chosen differently.

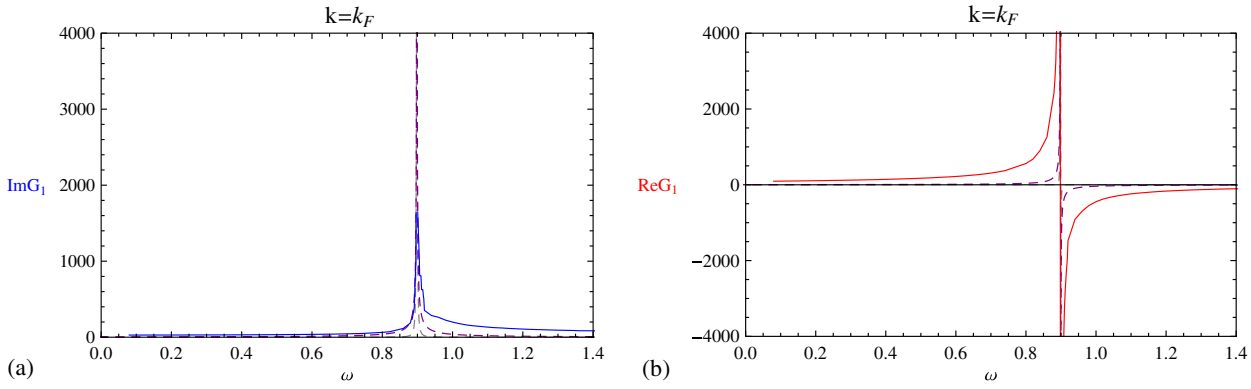

FIG. 9 (color online). $k = k_F$, both (a) and (b) with two fitting curves: (1) LFL Eq. (4.5) with $n = 2$ in the gray-dashed line, (2) LFL Eq. (4.5) with $n = 1$ in the purple-dashed line. At $k = k_F$, scaling ansatz of both forms Eq. (4.8) and Eq. (4.10) runs into trouble. We have not yet found a good fitting.

and larger decay rate $1/\tau_k \sim (\omega - \omega_F)^{2-\epsilon}$ than LFL $1/\tau_k \sim (\omega - \omega_F)^2$ close to Fermi energy ω_F. Compared to LFL, the quasiparticle description of Schrödinger Fermi liquids is less robust.

(3) Near the pole location, we have not found a promising fitting for Senthil's ansatz for both sides of $\omega > \omega_F$ and $\omega < \omega_F$.

1. $k < k_F$

For $k < k_F$, our scaling ansatz is[12]

$$\frac{c_0(k-k_F)^{-\alpha}}{\log(\frac{-(\omega-\omega_F)}{c_1(k-k_F)^z}) + i\gamma_0}. \tag{4.8}$$

[12]For $\omega < \omega_F$ under $k < k_F$, the term inside logarithmic becomes negative, where we choose the complex logarithm as follows:

$$\frac{c_0(k-k_F)^{-\alpha}}{\log(\frac{(\omega-\omega_F)}{c_1(k-k_F)^z}) + i\pi + i\gamma_0}. \tag{4.7}$$

2. $k > k_F$

For $k > k_F$, our scaling ansatz is[13]

$$\frac{c_0(k-k_F)^{-\alpha}}{\log(\frac{-(\omega-\omega_F)}{c_1(k-k_F)^z}) - i\gamma_0}. \tag{4.10}$$

3. $k = k_F$.

LFL fitting must be symmetric with respect to $\omega = \omega_F$ at $k = k_F$ for $\mathrm{Im}\, G_1$; however, the $\mathrm{Im}\, G_1$ from Schrödinger Fermi liquids is not symmetric along $\omega = \omega_F$. This is the major difference.

[13]For $\omega > \omega_F$ under $k > k_F$, the term inside logarithmic becomes negative, where we choose the complex logarithm as follows:

$$\frac{c_0(k-k_F)^{-\alpha}}{\log(\frac{(\omega-\omega_F)}{c_1(k-k_F)^z}) - i\pi - i\gamma_0}. \tag{4.9}$$

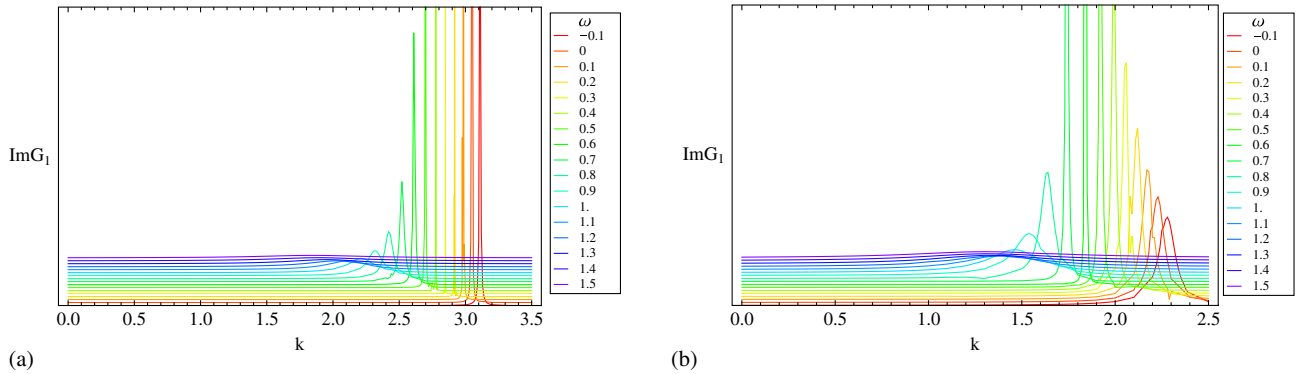

FIG. 10 (color online). $\mathrm{Im}\, G_1$ of Schrödinger Fermi liquids for $\beta > \beta^*$: (a) $\beta = 2$; (b) $\beta = 1$.

V. FERMIONIC QUANTUM PHASE TRANSITION

The Schrödinger black hole introduces two additional parameters to the nonrelativistic conformal background, other than the parameters which occurred already in asymptotic AdS spacetime [10]. The first parameter is the mass operator M(particle number eigenvalue), the second one is background density β.[14] In the zero temperature phase, a natural question arises: what happened to the Fermi surface if background density β is tuned? We should fix M while varying β.[15] In Sec. V A, we encounter again the phase with Fermi surfaces, gradually tune down β near $1/2$; we find a critical point (or critical line) in Sec. V B. Smaller β shows that Fermi surface collapses and then disappears in Sec. V C. Altogether this may indicate a quantum phase transition of fermionic liquids.

A. Well-defined Fermi surface ($\beta > \beta^*$)

When $\beta > 1/2$, an obvious peak appears in Im G_1, see Fig. 10. Analytically the peak should approach $\delta(k - k_F, \omega - \omega_F)$ at (k_F, ω_F). However, the numerical value $\mathrm{Im}\, G_1(k_F, \omega_F)$ cannot really be infinite. What we find is that the peak $\mathrm{Im}\, G_1(k_F, \omega_F)$ values in this region $\beta > 1/2$ depends on the finite IR cutoff. The smaller the initial cutoff $\epsilon = r - 1$, the larger the numerics $\mathrm{Im}\, G_1(k_F, \omega_F)$ at the peak grows. This is a sign for the suppose-to-be infinite pole. The pole of $\mathrm{Im}\, G_1$ indicates a well-defined Fermi surface. At larger β, the pole and nearby region on the (k, ω) plane develops much sharper. Notice that the pole shifts to larger ω_F and smaller k_F by decreasing β.

B. Near the quantum critical point ($\beta \simeq \beta^*$)

As β approaches in the range between $1/\sqrt{2}$ and $1/2$, we find the $\mathrm{Im}\, G_1(k_F, \omega_F)$ peak becomes insensitive to IR finite cutoff ϵ, the peak values are lower for smaller β, shown in Fig. 11. The stable peak value indicates there is no δ-function-like pole on the (k, ω) plane. By tuning β to a smaller value, the Fermi surface gradually collapses and disappears. We interpret the physics as

$$\beta > 1/2, \qquad \mathrm{Im}\, G_1(k_F, \omega_F) \simeq Z\delta(k - k_F, \omega - \omega_F) + \text{finite terms}, \quad \text{where } Z \neq 0. \tag{5.1}$$

$$\beta \simeq 1/2, \qquad \mathrm{Im}\, G_1(k_F, \omega_F) \simeq Z\delta(k - k_F, \omega - \omega_F) + \text{finite terms}, \quad \text{with} \quad Z \to 0. \tag{5.2}$$

Since the Z goes to zero at finite $\beta \simeq 1/2$, we suspect it is not a smooth crossover behavior. We expect a quantum critical point β^* (or quantum critical line) slightly larger than $\beta = 1/2$, and smaller than $\beta = 1/\sqrt{2}$. For convenience, we denote $\beta^* \simeq 1/2$, as in Fig. 11. We do not numerically determine β^* due to the computational limitation. A more detailed scan near the peak at $\beta \simeq 1/2$ may determine the exact value of β^*.

[14]Usually a quantum phase transition is tuned by a dimensionless coupling [16]; in our case we can define the coupling $g_\beta \equiv \beta\sqrt{\mu_Q}$ with μ_Q fixed in our case. Since the Hamiltonian description of boundary theory is unknown, we schematically tune β to address the same physics as tuning g_β.

[15]Here we tune β with various values $1/16$, $1/4$, $1/2$, $1/\sqrt{2}$, 1, 2, 8. The other parameters should be fixed. We choose $M = \ell' + qQ\beta$ fixed to be $1/10$, $T = 0(Q = \sqrt{2})$, $\Delta_\pm(\nu_\pm)$ is fixed by $m = 1/10$ and M. Among all the five parameters of the system, the remaining parameter μ_Q is subtle, which is $\mu_Q = Q/(2\beta)$. In our numerics, we choose to fix $q = 1$, in this case it seems like chemical potential μ_Q varies while β is tuned. One may argue that a resolution is considering $\mu_q \equiv q\mu_Q$, where μ_q is still allowed to be fixed while q compensates to be adjusted correspondingly. This resolution seems to fix the (chemical potential) energy to add a fermion of charge q into the system. However, we should be aware that in any case the chemical potential μ_Q is indeed varied. In addition, the "real" chemical potential to set the scale of Fermi energy μ_F is not merely as in [10] only μ_q alone. In our Schrödinger system, the Fermi energy should be identified by the coordinate $\tilde{\omega}$, the Fermi energy μ_F is set by $\tilde{\omega} + \mu_F = (\beta(\omega + qA_t) + (l - qA_\xi)/(2\beta))|_\partial = \tilde{\omega}$. This shows that $\mu_F = q(\beta A_t - A_\xi/(2\beta))|_\partial = 0$ is independent of β. Therefore, Fermi energy $\mu_F = 0$ is already fixed. We choose to fix the charge q of fermionic contents, instead of varying fermion charge q to fix the energy μ_q of inserting a fermion.

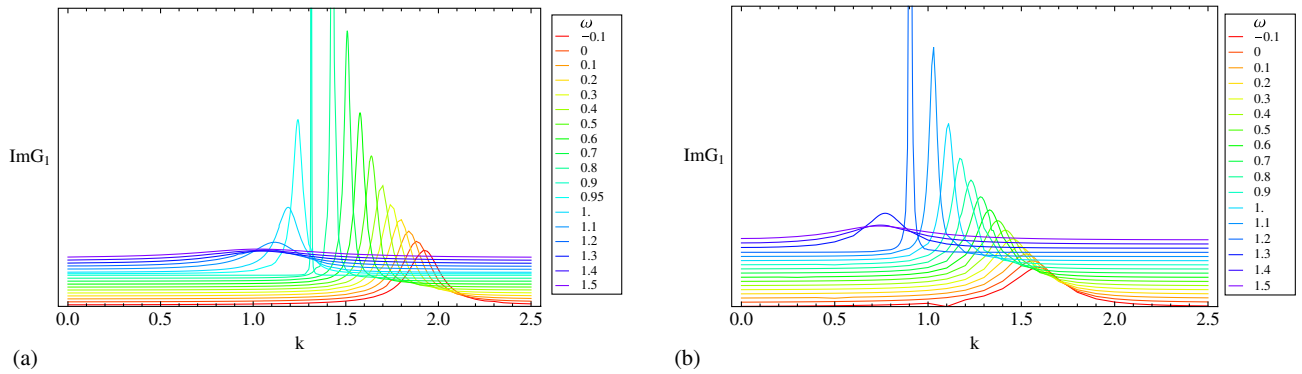

FIG. 11 (color online). $\mathrm{Im}\, G_1$ of Schrödinger Fermi liquids near β^*: (a) $\beta = 1/\sqrt{2}$; (b) $\beta = 1/2 \simeq \beta^*$.

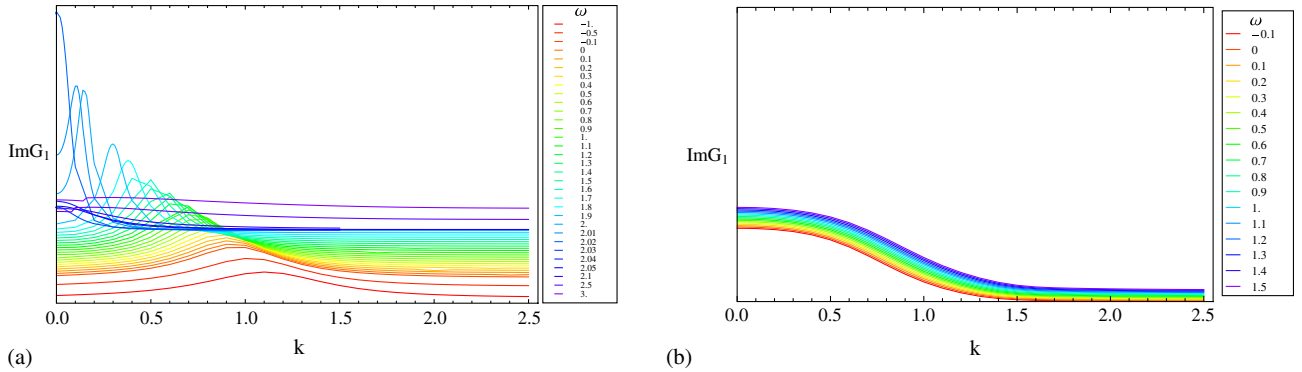

FIG. 12 (color online). $\mathrm{Im}\, G_1$ of Schrödinger Fermi liquids for $\beta < \beta^*$: (a) $\beta = 1/4$; (b) $\beta = 1/16$.

C. Fermi surface collapse and disappearance ($\beta < \beta^*$)

At smaller $\beta < 1/2$, we find no sharp peak but only a smoother hump. Unlike the Mott insulator for Mott transition [33,34], we do not have gaps opened up in $A(k,\omega)$. Indeed $A(k,\omega)$ does not dip to zero in this phase. There is no nonanalyticity in $A(k,\omega)$ to pinpoint k_F. This shows it is still a gapless phase but with Fermi surface disappearance. We show a series of $\mathrm{Im}\, G_1$ plots by varying β in Figs. 10–12. Note that the vertical axes for $\mathrm{Im}\, G_1$ shows no tick marks, we only show a landscape scanning through many slices of $\mathrm{Im}\, G_1$. Each slice of $\mathrm{Im}G_1(k,\omega)$ has a fixed ω, and scanning k values. Each slice of $\mathrm{Im}\, G_1$ has been shifted vertically for a clear vision of the landscape. As in footnote 11, we had discussed the L_ξ size of the compact ξ circle modifies $\mathrm{Im}\, G_1$ to the physical value of $A(k,\omega)$. Therefore, here the exact value of $\mathrm{Im}\, G_1$ is immaterial; only the relative height of $\mathrm{Im}\, G_1$ matters.

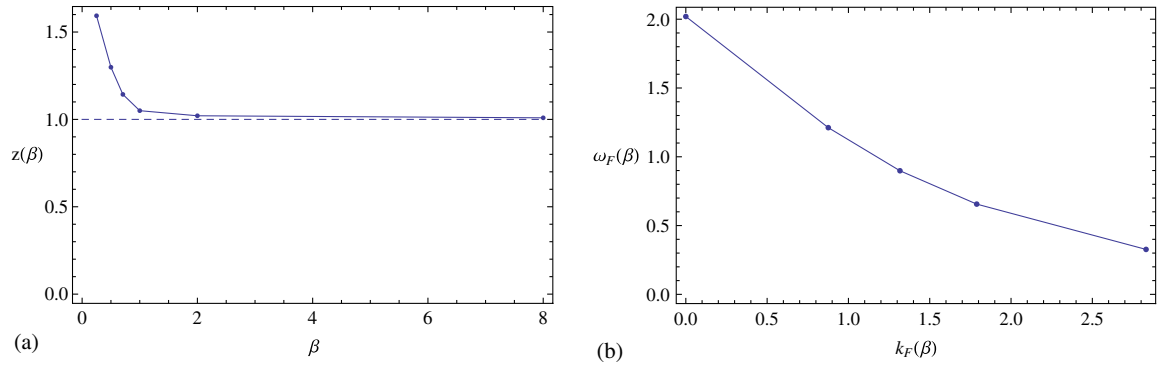

FIG. 13 (color online). (a) The relation between z and β for six data points are: $\beta = 1/4$, $z = 1.593$, $\beta = 1/2$, $z = 1.299$, $\beta = 1/\sqrt{2}$, $z = 1.143$, $\beta = 1$, $z = 1.050$, $\beta = 2$, $z = 1.021$, $\beta = 8$, $z = 1.009$. (b) For various $\beta = 1/4, 1/2, 1/\sqrt{2}, 1, 2$, the Fermi momentum and energy (k_F, ω_F) are (0.0000303, 2.020), (0.8762, 1.212), (1.317, 0.8984), (1.789, 0.656), (2.8304, 0.3266).

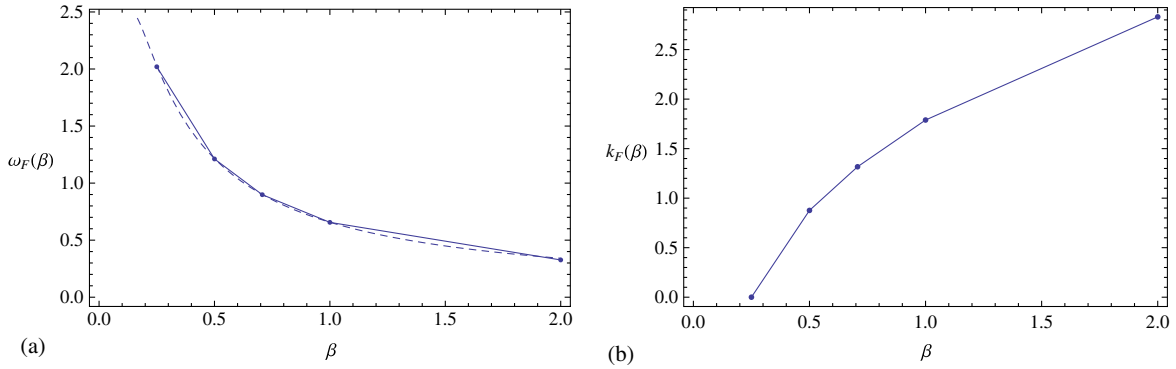

FIG. 14 (color online). (a) The location of the $\mathrm{Im}[G_1]$ peak at ω_F varies with respect to β. The numerical data points compared to the dashed curve fitting $\omega_F(\beta) = -(M - qQ\beta)/(2\beta^2)$. (b) The location of the Fermi-momentum k_F varies with respect to β.

D. Evolutions of dynamical exponent z and Fermi-momentum k_F under tuning background density β

Here we study the evolutions of the dynamical exponent z, Fermi energy ω_F, and Fermi-momentum k_F while tuning β in Figs. 13 and 14. When $\beta \lesssim \beta^*$, there is no good quasiparticle description for the system, so in which case (ω_F, k_F) means the (ω, k) coordinates of the highest peak in spectral function, z just means the dispersion reading from the branches structure around the highest peak.

In all of the data above, $\alpha \simeq 1.00$, thus our data follows the general relation $z \geq \alpha$ and $z \geq 1$ as Senthil's argument [33,34]. As β increases, z goes close to 1. Tentatively it suggests a more Landau Fermi liquids like behavior at the large β limit. Though from the spectral density fitting, we find the imaginary part of quasiparticle does not obey $\gamma(\omega) \propto \omega^2$ and $\mathrm{Im}[G_1(k,\omega)]$ near k_F is not symmetric with respect to ω_F. These two features are distinct from LFL. The large β limit is at most a close cousin of LFL.

In Sec. IV A, we showed $\omega_F = -\ell/(2\beta^2)$. In the case of tuning β while fixing the mass operator $\ell - qM_o = \ell + qQ\beta = M$, we expect $\omega_F(\beta) = -(M - qQ\beta)/(2\beta^2)$. We show this power law fitting agrees with our data in Fig. 14. On the other hand, the Fermi-momentum k_F requires better understanding of UV physics; we do not have a fitting here.

VI. CONCLUSION AND OPEN QUESTIONS

In summary, we have studied a class of strongly interacting nonrelativistic fermions under asymptotic NRCFT background in $2+1$D. We make some efforts to deal with the aforementioned two shortcomings of AdS space. First, our model has a better realization of nonrelativistic properties of many-body systems, and we have observed the well-defined Fermi surface of Schrödinger Fermi liquids. Second, by tuning the background density β with fixed particle number M, we realized a fermionic quantum phase transition as Fig. 15, where the larger β side shows a sharp Fermi surface, while the smaller β side shows Fermi surface disappearance. We find Senthil's scaling ansatz generally a better fit than Landau Fermi liquid (LFL) to our non-Fermi liquids. Based on quasiparticle self-energy scaling, we argue the quasiparticle description of Schrödinger Fermi liquids has shorter lifetime and is less stable comparing to LFL.

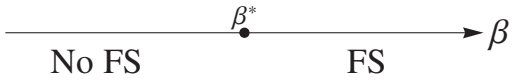

FIG. 15. The zero T quantum phase transition diagram of Schrödinger Fermi liquids. A phase with Fermi surface (FS) appears in $\beta > \beta^*$. A quantum critical region near $\beta \simeq \beta^*$ (it is undetermined yet whether β^* is a critical point or critical line, and unknown whether the transition is 1st order or higher order). A phase without Fermi surface appears in $\beta < \beta^*$. Note to tune a dimensionless coupling g_β, we can define $g_\beta \equiv \beta\sqrt{\mu_Q}$ with μ_Q fixed.

We leave some questions for future directions: (1) Quasiparticle residue Z may be regarded as the order parameter for the quantum phase transition. How does Z in Eq. (5.1) behave near the quantum critical point (or line); what is the order of phase transition? We have not yet been able to answer these questions. It will be illuminating to understand whether Schrödinger Fermi liquids shows discontinuous 1st, or continuous 2nd order or higher order transition, and the possibility to realize similar phase transitions proposed in [33,34]. It is also noteworthy that the location of poles has been captured very well analytically by the speculated curve $\omega_F(\beta) = -(M - qQ\beta)/(2\beta^2)$ as in Fig. 14, though we see numerical data slightly deviated from the analytic curve (at three digits after the decimal mark). It will be important to know the physical mechanism or subleading corrections for this deviation.

(2) Notably the charge or particle number U(1) symmetry are unbroken in our probe limit. Fermi surface and gauge-gravity duality relation are mentioned in [44,45], especially the relation between a global U(1) symmetry and the existence of Fermi surface. How does our system realize

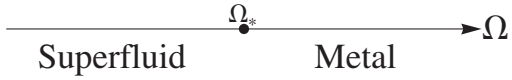

FIG. 16. Bosonic quantum phase transition is likely found at low temperature phase in [30]. On the large background density ($\Omega > \Omega_*$) side, the phase is in the metallic state with unbroken U(1) symmetry. On the smaller background density ($\Omega < \Omega_*$) side, there shows a superfluid phase with broken U(1) symmetry. Note to tune a dimensionless coupling g_Ω, we can define $g_\Omega \equiv \Omega/\sqrt{\mu_Q}$ with μ_Q fixed.

a quantum phase transition with Fermi surface disappearance without breaking global U(1) symmetry or translational symmetry? Our attention is brought to an earlier work [30], where we consider a toy model of bosonic system under asymptotic NRCFT, where a U(1) symmetry is broken by condensed boson fields around the Schrödinger black hole. The bosonic quantum phase transition is likely found there at low temperature phase as Fig. 16. It is unavoidable to ask whether these two phase transitions in Figs. 15 and 16 have any similar nature. On one side, $\beta > \beta^*$ of Fig. 15 shows a conducting phase with Fermi surface with unbroken U(1) symmetry; the $\Omega > \Omega_*$ side of Fig. 16 shows a metallic state with unbroken U(1) symmetry. On the other side, $\beta < \beta^*$ of Fig. 15 shows Fermi surface disappearance; the $\Omega < \Omega_*$ side of Fig. 16 shows a superfluid state with broken U(1) symmetry. Though the two systems have similar asymptotic NRCFT background, one should be aware that the two systems are rather different. The bulk side of the fermionic model has a charged Schrödinger black hole, where the gauge field is chosen to be fixed, the Dirac fermion is in a probe limit. On the other hand, the bulk side of the bosonic model in [30] has a neutral Schrödinger black hole, where both the gauge field and bosons are in a probe limit. The comparison with a Hawking-Page-like transition such as [46] would be interesting. Another possible future direction is studying the effective Schrödinger potential with the density β dependence along the lines of [47–49].

(3) It will be illuminating to address more about the phase with Fermi surface disappearance. In the phase without Fermi surface, there is no superconducting gap opened up in the spectral function. Specifically we do not introduce any pairing term (such as Yukawa spinor-scalar pairing) in the bulk action, so it is not a superconducting phase.[16] We only can suspect that tuning β from large to small effectively implies tuning fermion interaction from weaker coupling to stronger coupling—from more Fermi-liquid-like ($z \simeq 1$) to non-Fermi liquids ($z > 1$) to strongly correlation smear the $A(k, \omega)$ discontinuity into continuity near ω_F, k_F. Whether one can understand more about the nature of this Fermi surface disappearance, we leave this for future study.

(4) It is of considerable interest to perform rigorous holographic renormalization for spinors to justify the holographic dictionary of Green's function, following [28,37,38]. The issue of the proposed counterterms, being totally local [28] or nonlocal [37], has not found complete agreement in the literature. We remark that the discrepancy in holographic renormalization seems to persist and remains to be satisfactorily resolved.

On the other hand, a subtle issue is that the conformal dimensions Δ of Schrödinger spinors have $\nu_\pm$ with peculiar $m \pm 1/2$ dependence, distinct from the AdS case [10,32]. In the AdS case, there are two sets of two component spinors (in [10,32] notation, D and A for the standard quantization, B and C for the alternate quantization). In the Schrödinger case, there are doubled sectors, i.e. ν_+ sectors (as $\mathbf{S}_1$, $\mathbf{R}_1$) and ν_- sectors (as $\mathbf{S}_2$, $\mathbf{R}_2$) shown in Eqs. (3.7) and (3.8). There is only one independent parameter left for each projected spinor in each sector. One may wonder why the Green's function in the Schrödinger case does not possess the two-component spinor structure as in the AdS case? We emphasize that Green's function with two-component spinor structure (such as the result of [27]) has two problems. First, it is known that the (two-component) spinor structure does not appear in a free nonrelativistic fermion theory (analogous to nonrelativistic bosons) as discussed in [28]. At this level, [28] and our work find an agreement—there is no apparent gamma matrices/spinor structure in the final two-point fermionic Green's function. The second problem is that we find that this approach will sacrifice the distinction between the standard quantization and the alternate quantization, which is unreasonable. These two known issues seem to suggest our dictionary is a sensible approach.

While we may not have the final word in the correct prescription, our results show very interesting physical features, in particular the numerical results for the Fermi frequency matches closely an analytic guess based on physical reasoning. This should be another piece of supporting evidence that we are capturing the correct physics.

(5) Our model is a $2 + 1$D fermionic system. It will be important to study a system in $3 + 1$D which may exhibit fermions at unitarity [19,20]. It will also be interesting to explore dynamical exponents other than $z = 2$. Indeed gravity duals of finite density systems with asymptotic Schrödinger isometry for $d \neq 2$, $z \neq 2$ are known [23,52,53].

(6) The Schrödinger black hole at zero temperature has finite entropy, which implies that our theory may not describe a unique ground state but an ensemble of low energy states. Moreover, it has been pointed out that discrete light-cone quantization and β deformation from the parent AdS black hole [22–24,54,55] causes peculiar free energy scaling $F \sim -T^4/\mu^2$ for the system. It will be

[16] A setup along [50,51] is the next-step toward boson-fermion interaction, with a superconducting state under NRCFT background.

interesting to know whether bosons or fermions with a full consideration of spacetime backreaction can change the physics of our study, especially the IR AdS^2 geometry.

(7) It will be interesting to explore the electron star [56–59] in the context of Schrödinger asymptotic geometry.

ACKNOWLEDGMENTS

We would like to thank A. Adams, G. Baskaran, L. Y. Hung, N. Iqbal, H. Liu, R. Mahajan, J. McGreevy, D. Mross, Y. Nishida, K. Rajagopal, T. Senthil, D. Vegh, and W. Witczak-Krempa for valuable discussions. This work is supported by the U.S. Department of Energy under cooperative research agreement Contract No. DE-FG02-05ER41360 and NSF Grants No. DMR-1005541, No. NSFC 11074140, and No. NSFC 11274192. Research at Perimeter Institute is supported by the Government of Canada through Industry Canada and by the Province of Ontario through the Ministry of Research.

APPENDIX A: AdS_2 SCALING

The near horizon geometry of the charged Schrödinger black hole can be obtained by taking $r = r_0 + \epsilon$, with the coordinate redefinition:

$$\tilde{\tau} = K_0^{-1/3}\left(\tau + \frac{\beta^2 r_0^2}{1+\beta^2 r_0^2} y\right), \qquad \tilde{y} = \frac{K_0^{1/6}}{\sqrt{12}} y, \qquad \tilde{x_i} = \frac{K_0^{-1/3}}{\sqrt{12}} x, \tag{A1}$$

where $K_0 = (1+\beta^2 r_0^2)^{-1}$. The metric is

$$ds^2 = -\epsilon^2 d\tilde{\tau}^2/R_{AdS_2}^2 + R_{AdS_2}^2(d\epsilon^2/\epsilon^2) + r_0^2(d\tilde{y}^2 + d\tilde{x_1}^2 + d\tilde{x_2}^2)/R_{AdS_2}^2, \tag{A2}$$

with $R_{AdS_2} = \frac{(1+\beta^2 r_0^2)^{1/6}}{\sqrt{12}} R = \frac{K_0^{-1/6}}{\sqrt{12}} R$, which is $AdS_2 \times \mathbb{R}^3$ metric. The gauge field near horizon is $A = A_\tau d\tau = (A_\tau K_0^{1/3}) d\tilde{\tau} + (-A_\tau \beta^2 r_0^2 K_0^{5/6}\sqrt{12}) d\tilde{y}$, with $A_\tau \simeq \frac{2Q}{R^2 r_0^3}\epsilon = \frac{Q K_0^{-1/3}}{6 R_{AdS_2}^2 r_0^3}\epsilon$. One can solve the Dirac equation, with this AdS_2 background and supporting gauge field. We take the AdS_2 rescaling as in [26], send $\tau \to \tau/\lambda$ and $\epsilon \to \lambda\epsilon$ with $\lambda \to 0$. In this case, the Dirac equation near the AdS_2 boundary becomes

$$\left(\frac{\epsilon}{R_{AdS_2}}\Gamma_r \partial_\epsilon + \frac{1}{2R_{AdS_2}}\Gamma_r + C_{\tilde{\tau}}\Gamma_\tau + C_{\tilde{y}}\Gamma_y + C_{\tilde{x_1}}\Gamma_{x_1} - m\right)\psi = 0. \tag{A3}$$

Rewrite the above in terms of two sets of two-component spinors and "square" the operator to make it a second order differential equation; we find the "AdS_2" scaling dimension is the exponent ν of $\psi \propto \epsilon^{-\frac{1}{2}\pm\nu}$:

$$\nu = R_{AdS_2}\sqrt{m^2 + C_{\tilde{\tau}}^2 - C_{\tilde{y}^2} - C_{\tilde{x_1}^2}} \tag{A4}$$

with $C_{\tilde{\tau}} = -i\frac{qQ}{6r_0^3 R_{AdS_2}}$, $C_{\tilde{y}} = iR_{AdS_2}\sqrt{12}K_0^{-1/6}(-\beta\omega + \frac{\ell}{2\beta})$, $C_{\tilde{x_1}} = iR_{AdS_2} k\sqrt{12}K_0^{1/3}$.

APPENDIX B: NUMERICAL SETUP FOR GREEN'S FUNCTION

For the foreseeing convenience, we define a matrix Dm, which satisfies the Dirac equation Eq. (2.10), $\phi' \equiv \partial_r \phi = \mathrm{Dm}\phi$,

$$\mathrm{D_m} \equiv \frac{1}{r\sqrt{f}}\begin{pmatrix} mK^{-1/6} & 0 & -u-v & -ik/r \\ 0 & mK^{-1/6} & -ik/r & -u+v \\ -u+v & ik/r & -mK^{-1/6} & 0 \\ ik/r & -u-v & 0 & -mK^{-1/6} \end{pmatrix}. \tag{B1}$$

We define a converting matrix $\mathrm{C_v}$ as a function of r as

$$\mathrm{C_v} \equiv r^{1/2}\begin{bmatrix} r^{\nu_+-1}(a_{1+}+a_{2+}r^{-2}) & r^{-\nu_+-1}(\alpha_{1+}+\alpha_{2+}r^{-2}) & r^{\nu_-}(b_{1+}+b_{2+}r^{-2}) & r^{-\nu_-}(\beta_{1+}+\beta_{2+}r^{-2}) \\ r^{\nu_+-1}(a_{1-}+a_{2-}r^{-2}) & r^{-\nu_+-1}(\alpha_{1-}+\alpha_{2-}r^{-2}) & r^{\nu_-}(b_{1-}+b_{2-}r^{-2}) & r^{-\nu_-}(\beta_{1-}+\beta_{2-}r^{-2}) \\ r^{\nu_+}(c_{1+}+c_{2+}r^{-2}) & r^{-\nu_+}(\gamma_{1+}+\gamma_{2+}r^{-2}) & r^{\nu_--1}(d_{1+}+d_{2+}r^{-2}) & r^{-\nu_--1}(\delta_{1+}+\delta_{2+}r^{-2}) \\ r^{\nu_+}(c_{1-}+c_{2-}r^{-2}) & r^{-\nu_+}(\gamma_{1-}+\gamma_{2-}r^{-2}) & r^{\nu_--1}(d_{1-}+d_{2-}r^{-2}) & r^{-\nu_--1}(\delta_{1-}+\delta_{2-}r^{-2}) \end{bmatrix} \tag{B2}$$

and a set of functions $\mathbf{S_1}(r)$, $\mathbf{S_2}(r)$, $\mathbf{R_1}(r)$, $\mathbf{R_2}(r)$ can be defined from Eq. (3.20). This field-redefinition $\mathbf{S_1}(r)$, $\mathbf{S_2}(r)$, $\mathbf{R_1}(r)$, $\mathbf{R_2}(r)$ goes to $\mathbf{S_1}$, $\mathbf{S_2}$, $\mathbf{R_1}$, $\mathbf{R_2}$ at $r \to \infty$.

The EOM of $\mathbf{G}(r)$ in the bulk gravity is $\mathbf{G}'(r) = \mathbf{R}'(r)\mathbf{S}(r)^{-1} - \mathbf{G}(r)\mathbf{S}(r)'\mathbf{S}(r)^{-1}$. Apply Eqs. (B1) and (3.20), then $\mathbf{S}'(r)$ and $\mathbf{R}'(r)$ can be simplified in terms of the linear combination of $\mathbf{S}(r)$ and $\mathbf{R}(r)$:

$$\begin{aligned}[S_1'(r)R_1'(r)S_2'(r)R_2'(r)]^{\mathrm{T}} &= (\mathrm{C_v}^{-1}\phi(r))' \\ &= (\mathrm{C_v}^{-1}\,\mathrm{D_m}\,\mathrm{C_v} - \mathrm{C_v}^{-1}\mathrm{C_v}') \\ &\quad \times [\mathbf{S_1}(r)\mathbf{R_1}(r)\mathbf{S_2}(r)\mathbf{R_2}(r)]^{\mathrm{T}}.\end{aligned} \tag{B3}$$

The matrix $D_g(r) \equiv \mathrm{C_v}^{-1}\,\mathrm{D_m}\,\mathrm{C_v} - \mathrm{C_v}^{-1}\mathrm{C_v}'$ simplifies EOM to

$$\begin{aligned}\mathbf{G}'(r) = &\begin{bmatrix} D_{g2,1} & D_{g2,3} \\ D_{g4,1} & D_{g4,3} \end{bmatrix} + \begin{bmatrix} D_{g2,2} & D_{g2,4} \\ D_{g4,2} & D_{g4,4} \end{bmatrix} \cdot \mathbf{G}(r) \\ &- \mathbf{G}(r) \cdot \left(\begin{bmatrix} D_{g1,1} & D_{g1,3} \\ D_{g3,1} & D_{g3,3} \end{bmatrix} + \begin{bmatrix} D_{g2,1} & D_{g2,3} \\ D_{g4,1} & D_{g4,3} \end{bmatrix} \cdot \mathbf{G}(r) \right).\end{aligned} \tag{B4}$$

Numerically we solve this bulk EOM [Eq. (B4)] of the Green's function with the initial condition to obtain physical results of Eq. (3.26).

Our program code for numerical computation is shared through Supplemental Material [35].

APPENDIX C: HOLOGRAPHIC DICTIONARY FOR THE ALTERNATIVE QUANTIZATION

In Sec. III A, we set up the holographic dictionary for the standard quantization. Here we also walk through the similar setup for the alternative quantization. Consider the subleading term of ϕ_- contributes as a source field, then

$$\psi_- = (-gg^{rr})^{-1/4}\phi_- \simeq r^{-2}\phi_- \simeq S_2 D_1 r^{\nu_- - 5/2} \tag{C1}$$

which corresponds to the source χ_-,

$$\chi_- = \lim_{r\to\infty} r^{\frac{5}{2}-\nu_-}\psi_- \simeq \mathbf{S_2} D_1. \tag{C2}$$

χ_- is proportional to $\mathbf{S_2}$. The momentum field $\bar{\Pi}_-$ is

$$\begin{aligned}\bar{\Pi}_- &= \sqrt{-gg^{rr}}\psi_+ = (-gg^{rr})^{1/4}\phi_+ \\ &\simeq r^2\phi_+ \simeq \mathbf{S_2}B_1 r^{\nu_- + 5/2} + \mathbf{R_2}\beta_1 r^{-\nu_- + 5/2} + \cdots\end{aligned} \tag{C3}$$

which corresponds to the response $\mathcal{O}_-$,

$$\bar{\mathcal{O}}_- = \lim_{r\to\infty} r^{\nu_- - \frac{5}{2}}\bar{\Pi}_- \simeq \mathbf{R_2}\beta_1. \tag{C4}$$

$\mathcal{O}_-$ is proportional to $\mathbf{R_2}$. On the other hand, we can go through the same logic again, though consider the subleading term of ϕ_+ contributes as a source field, then

$$\psi_+ = (-gg^{rr})^{-1/4}\phi_+ \simeq r^{-2}\phi_+ \simeq \mathbf{S_1}A_1 r^{\nu_+ - 5/2} \tag{C5}$$

which corresponds to the source χ_+,

$$\chi_+ = \lim_{r\to\infty} r^{\frac{5}{2}-\nu_+}\psi_+ \simeq \mathbf{S_1}A_1. \tag{C6}$$

χ_+ is proportional to $\mathbf{S_1}$. The momentum field $\bar{\Pi}_+$ is

$$\begin{aligned}\bar{\Pi}_+ &= -\sqrt{-gg^{rr}}\psi_- \\ &= -(-gg^{rr})^{1/4}\phi_- \simeq -r^2\phi_- \simeq -S_1 C_1 r^{\nu_+ + 5/2} \\ &\quad - R_1\gamma_1 r^{-\nu_+ + 5/2} + \cdots\end{aligned} \tag{C7}$$

which corresponds to the response $\mathcal{O}_+$,

$$\mathcal{O}_+ = -\lim_{r\to\infty} r^{\nu_+ - \frac{5}{2}}\bar{\Pi}_+ \simeq R_1\gamma_1. \tag{C8}$$

$\mathcal{O}_+$ is proportional to $\mathbf{R_1}$. Now we again derive $\mathbf{S_1}$, $\mathbf{S_2}$ are identified as sources, $\mathbf{R_1}$, $\mathbf{R_2}$ are identified as responses for this alternative quantization.

APPENDIX D: PURE SCHRÖDINGER GREEN'S FUNCTION AT ZERO T ZERO DENSITY

1. Two-point correlators at the leading order

Here we compare the pure Schrödinger two-points function at zero T zero density of Ref. [27] with our formulation.[17] Specifically, in $d = 2$, they show

$$\langle \psi_M(x,t)\bar{\psi}_M(0,0)\rangle \propto r^{2\nu_+}. \tag{D1}$$

Here we cross-check our analysis indeed matches theirs. The boundary action is $\int_{\partial\mathcal{M}} dtd\xi d^2x\sqrt{-gg^{rr}}\bar{\psi}\psi$, with $\sqrt{-gg^{rr}} = r^4$, by plugging our UV boundary expansion in Eqs. (3.7) and (3.8), with $\psi = (-gg^{rr})^{-1/4}\phi \simeq r^{-2}\phi$, we arrive at $\bar{\psi}\psi|_{\partial\mathcal{M}} \propto r^{-4}\bar{\phi}\phi$. Notice Γ_τ in $\bar{\phi}\phi$ coupling the 1st to the 3rd component of ϕ, meanwhile coupling the 2nd to the 4th component of ϕ. With the leading piece in ϕ is $\mathbf{S_1}r^{\nu_+ + \frac{1}{2}}$. This couples to the leading order of the 2nd component of ϕ, which is $\mathbf{S_1}r^{\nu_+ - \frac{1}{2}}a_2$. Neglecting other factors and coefficients,

$$\int_{\partial\mathcal{M}} dtd\xi d^2x\sqrt{-gg^{rr}}\bar{\psi}\psi \propto \bar{\phi}\phi \propto r^{2\nu_+}. \tag{D2}$$

One can obtain the scaling form of two-point correlator $\langle \psi_M(x,t)\bar{\psi}_M(0,0)\rangle$ at the leading order $r^{2\nu_+}$. The scaling $r^{2\nu_+}$ matches for Refs. [27] and [28] and our works,

[17] In [27], their ϵ coordinates are inverse of our r, also their $d = 3$ is our $d = 2$ case.

however the precise form of our correlator is *not* identical with Ref. [27]. We should note that both Ref. [28] and our work contain higher order terms in the fermion field source/response, thus both works contain $r^{2\nu_+}$, $r^{2\nu_-}$ scaling, while Ref. [27] only contains $r^{2\nu_+}$ scaling. In the next subsection, we will delve further into our Green's function and its similarity with that of Ref. [28].

2. Pure Schrödinger Green's function from response over source

Solve the Dirac's equation in zero T zero density Schrödinger spacetime $ds^2 = -r^4dt^2 + 2r^2dtd\xi + r^2d\vec{x}^2 + dr^2/r^2$, the bulk fields have the following form:

$$\psi_+ = r^{-\frac{d+3}{2}}K_{\nu_+}(\mathbf{k}/r)V^+ + g_+(\mathbf{k},r)\Gamma_\xi U^+ + r^{-\frac{d+3}{2}}K_{-\nu_+}(\mathbf{k}/r)V^- + g_-(\mathbf{k},r)\Gamma_\xi U^-, \tag{D3}$$

$$\psi_- = f_+(\mathbf{k},r)\Gamma_\xi V^+ + r^{-\frac{d+3}{2}}K_{\nu_-}(\mathbf{k}/r)U^+ + f_-(\mathbf{k},r)\Gamma_\xi V^- + r^{-\frac{d+3}{2}}K_{-\nu_-}(\mathbf{k}/r)U^-, \tag{D4}$$

where d is the spatial dimension of $\vec{x}$, and the quantity

$$\mathbf{k} = \sqrt{-2\ell\omega + k^2}$$

is a coordinate-invariant form of momentum. We denote U^+, V^+ as two components spinor bases for $\nu_\pm$ series (the first two columns), and denote U^-, V^- as two components spinor bases for $-\nu_\pm$ series (the last two columns), $K_\nu(\mathbf{k}/r)$ is modified Bessel function, solution of $r^2\partial_r^2K_\nu(\mathbf{k}/r) + r\partial_rK_\nu(\mathbf{k}/r) - ((\mathbf{k}/r)^2 + \nu^2)K_\nu(\mathbf{k}/r) = 0$. The expansions of $K_{\nu_\pm}(\mathbf{k}/r)$, $f_\pm(\mathbf{k},r)$, $g_\pm(\mathbf{k},r)$, ψ_+, ψ_- near $r\to\infty$ are

$$K_{\nu_\pm}(\mathbf{k}/r) = 2^{-1+\nu_\pm}(\mathbf{k}/r)^{-\nu_\pm}\Gamma(\nu_\pm)(1+O(r^{-2})), \tag{D5}$$

$$f_\pm(\mathbf{k},r) = i\frac{2^{\pm\nu_+-2}\ell\Gamma(\pm\nu_+)}{\pm\nu_+ + m + \frac{1}{2}}k^{\mp\nu_+}r^{-\frac{d+1}{2}\pm\nu_+}(1+O(r^{-2})), \tag{D6}$$

$$g_\pm(\mathbf{k},r) = -i\frac{2^{\pm\nu_--2}\ell\Gamma(\pm\nu_-)}{\pm\nu_- - m + \frac{1}{2}}k^{\mp\nu_-}r^{-\frac{d+1}{2}\pm\nu_-}(1+O(r^{-2})), \tag{D7}$$

$$\psi_+ = Ar^{\nu_+-\frac{d+3}{2}}(1+O(r^{-2})) + Br^{\nu_--\frac{d+1}{2}}(1+O(r^{-2})) + \alpha r^{-\nu_+-\frac{d+3}{2}}(1+O(r^{-2})) + \beta r^{-\nu_--\frac{d+1}{2}}(1+O(r^{-2})), \tag{D8}$$

$$\psi_- = Cr^{\nu_+-\frac{d+1}{2}}(1+O(r^{-2})) + Dr^{\nu_--\frac{d+3}{2}}(1+O(r^{-2})) + \gamma r^{-\nu_+-\frac{d+1}{2}}(1+O(r^{-2})) + \delta r^{-\nu_--\frac{d+3}{2}}(1+O(r^{-2})). \tag{D9}$$

Notice $\psi_+ = (-gg_{rr})^{-\frac{1}{4}}\phi_+$ and $\psi_- = (-gg_{rr})^{-\frac{1}{4}}\phi_-$, we can compare this expansion with respect to Eqs. (3.7) and (3.8). The expansion matches, with the projection constrains on the spinors:

$$C = \frac{-\ell}{2\beta(\nu_+ + m + \frac{1}{2})}P_-A, \qquad B = \frac{-\ell}{2\beta(\nu_- - m + \frac{1}{2})}P_+D, \tag{D10}$$

$$\gamma = \frac{-\ell}{2\beta(-\nu_+ + m + \frac{1}{2})}P_-\alpha, \qquad \beta = \frac{-\ell}{2\beta(-\nu_- - m + \frac{1}{2})}P_+\delta. \tag{D11}$$

In the case of the charged Schrödinger black hole for Eqs. (3.7) and (3.8), the projection relation Eq. (D10), Eq. (D11)'s ℓ is replaced by $\ell + qQ\beta$ for Eq. (3.10), Eq. (3.11).

There are extra constraints on two-component spinors $V^\pm$, $U^\pm$:

$$V^\pm = \frac{-i}{2\ell}(ik^\mu\Gamma_\mu)\Gamma_\xi V^\pm, \qquad U^\pm = \frac{-i}{2\ell}(ik^\mu\Gamma_\mu)\Gamma_\xi U^\pm, \tag{D12}$$

or equivalently,

$$\Gamma_\xi V^\pm = \frac{2\ell(k^\mu\Gamma_\mu)}{\mathbf{k}^2}V^\pm, \qquad \Gamma_\xi U^\pm = \frac{2\ell(k^\mu\Gamma_\mu)}{\mathbf{k}^2}U^\pm, \tag{D13}$$

where $k^\mu\Gamma_\mu = \ell\Gamma_t - \omega\Gamma_\xi + k_x\Gamma_x$. By identifying source and response based on our holographic dictionary, we have the response and source matrix,

$$\begin{aligned}\mathbf{R} &= \begin{bmatrix}\mathbf{R}_\mathbf{1}^1 & \mathbf{R}_\mathbf{1}^2\\ \mathbf{R}_\mathbf{2}^1 & \mathbf{R}_\mathbf{2}^2\end{bmatrix}\\ &= \begin{bmatrix}2^{-\nu_+-1}\Gamma(-\nu_+)\mathbf{k}^{\nu_+}(V^-)_2^{(1,2)}\\ 2^{-\nu_--1}\Gamma(-\nu_-)\mathbf{k}^{\nu_-}(U^-)_3^{(1,2)}\end{bmatrix}\\ &= \begin{bmatrix}2^{-\nu_+-2}\Gamma(-\nu_+)\mathbf{k}^{\nu_+}\frac{-i}{\ell}(ik^\mu\Gamma_\mu\Gamma_\xi V^-)_2^{(1,2)}\\ 2^{-\nu_--2}\Gamma(-\nu_-)\mathbf{k}^{\nu_-}\frac{-i}{\ell}(ik^\mu\Gamma_\mu\Gamma_\xi U^-)_3^{(1,2)}\end{bmatrix},\end{aligned} \tag{D14}$$

$$\mathbf{S}=\begin{bmatrix}\mathbf{S}_{\mathbf{1}}^{1} & \mathbf{S}_{\mathbf{1}}^{2}\\ \mathbf{S}_{\mathbf{2}}^{1} & \mathbf{S}_{\mathbf{2}}^{2}\end{bmatrix}=\begin{bmatrix} i\frac{2^{\nu_+-2}\ell\Gamma(\nu_+)}{\nu_++m+\frac{1}{2}}\mathbf{k}^{-\nu_+}(\Gamma_\xi V^+)_4^{(1,2)} \\ -i\frac{2^{\nu_--2}\ell\Gamma(\nu_-)}{\nu_--m+\frac{1}{2}}\mathbf{k}^{-\nu_-}(\Gamma_\xi U^+)_1^{(1,2)}\end{bmatrix}. \tag{D15}$$

Here we follow the notation in Sec. III C, introducing upper indices (1, 2) to distinguish the first and the second sets of two independent boundary conditions for spinors. We also introduce lower indices $j=1,2,3,4$, implying the jth component of 4-spinor. For example, $(V^+)_4^{(2)}$ means reading the fourth component of the spinor (V^+) from the second (2) type of boundary condition.

For the notation convenience, we define

$$\begin{aligned} V^{-(1,2)}&=(k^\mu\Gamma_\mu\Gamma_\xi V^-)_2^{(1,2)},\\ U^{-(1,2)}&=(k^\mu\Gamma_\mu\Gamma_\xi U^-)_3^{(1,2)},\end{aligned} \tag{D16}$$

$$V^{+(1,2)}=(\Gamma_\xi V^+)_4^{(1,2)},\qquad U^{+(1,2)}=(\Gamma_\xi U^+)_1^{(1,2)}. \tag{D17}$$

Again, the upper indices (1,2) are choices for the first or the second independent boundary conditions. The lower indices 1, 2, 3, 4 are indices for spinor components. Green's function is

$$\mathbf{G}=\begin{bmatrix}\mathbf{G}_{\mathbf{1}}^{1} & \mathbf{G}_{\mathbf{1}}^{2}\\ \mathbf{G}_{\mathbf{2}}^{1} & \mathbf{G}_{\mathbf{2}}^{2}\end{bmatrix} \tag{D18}$$

with each component

$$\mathbf{G}_{\mathbf{1}}^{1}=\frac{-i}{\ell^2}\left(\frac{\mathbf{k}}{2}\right)^{2\nu_+}\frac{\Gamma(-\nu_+)}{\Gamma(\nu_+)}\times\left(\nu_++m+\frac{1}{2}\right)\frac{(V^{-(1)}U^{+(2)}-V^{-(2)}U^{+(1)})}{(V^{+(1)}U^{+(2)}-V^{+(2)}U^{+(1)})}, \tag{D19}$$

$$\mathbf{G}_{\mathbf{1}}^{2}=\frac{i}{\ell^2}\left(\frac{\mathbf{k}}{2}\right)^{\nu_++\nu_-}\frac{\Gamma(-\nu_+)}{\Gamma(\nu_-)}\left(\nu_--m+\frac{1}{2}\right)\times\frac{(-V^{-(1)}V^{+(2)}+V^{-(2)}V^{+(1)})}{(V^{+(1)}U^{+(2)}-V^{+(2)}U^{+(1)})}, \tag{D20}$$

$$\mathbf{G}_{\mathbf{2}}^{2}=\frac{i}{\ell^2}\left(\frac{\mathbf{k}}{2}\right)^{2\nu_-}\frac{\Gamma(-\nu_-)}{\Gamma(\nu_-)}\left(\nu_--m+\frac{1}{2}\right)\times\frac{(-U^{-(1)}V^{+(2)}+U^{-(2)}V^{+(1)})}{(V^{+(1)}U^{+(2)}-V^{+(2)}U^{+(1)})}. \tag{D21}$$

$$\mathbf{G}_{\mathbf{2}}^{1}=\frac{-i}{\ell^2}\left(\frac{\mathbf{k}}{2}\right)^{\nu_++\nu_-}\frac{\Gamma(-\nu_-)}{\Gamma(\nu_+)}\left(\nu_++m+\frac{1}{2}\right)\times\frac{U^{-(1)}U^{+(2)}-U^{-(2)}U^{+(1)}}{(V^{+(1)}U^{+(2)}-V^{+(2)}U^{+(1)})}, \tag{D22}$$

We know that Green's function in [27] contains only the $r^{2\nu_+}$ contribution. Our two-point Green's function closely resembles that of Ref. [28] with subleading structure, $r^{2\nu_+}$, $r^{2\nu_-}$. A quick way to check this is comparing to Eq. (79) of [28], their $\langle\mathcal{O}_+^\dagger\mathcal{O}_+\rangle\simeq(k^2-2\ell\omega)^{\nu_+}$ scales identically as $\mathbf{G}_{\mathbf{1}}^{1}\sim\mathbf{k}^{2\nu_+}=(k^2-2\ell\omega)^{\nu_+}$ of ours, and their $\langle\mathcal{O}_-^\dagger\mathcal{O}_-\rangle\simeq(k^2-2\ell\omega)^{\nu_-}$ scales identically as $\mathbf{G}_{\mathbf{2}}^{2}\sim\mathbf{k}^{2\nu_-}=(k^2-2\ell\omega)^{\nu_-}$ of ours.

[1] S. Giorgini, L. P. Pitaevskii, and S. Stringari, Rev. Mod. Phys. **80**, 1215 (2008).
[2] I. Bloch, J. Dalibard, and W. Zwerger, Rev. Mod. Phys. **80**, 885 (2008).
[3] W. Ketterle and M. W. Zwierlein, in *Proceedings of the International School of Physics "Enrico Fermi,"* edited by M. Inguscio, W. Ketterle, and C. Salomon (IOS Press, Amsterdam, 2008), and references therein.
[4] Q. Si and F. Steglich, Science **329**, 1161 (2010).
[5] J. McGreevy, Physics **3**, 83 (2010).
[6] J. M. Maldacena, Adv. Theor. Math. Phys. **2**, 231 (1998); Int. J. Theor. Phys. **38**, 1113 (1999).
[7] S. S. Gubser, I. R. Klebanov, and A. M. Polyakov, Phys. Lett. B **428**, 105 (1998).
[8] E. Witten, Adv. Theor. Math. Phys. **2**, 253 (1998).
[9] S.-S. Lee, Phys. Rev. D **79**, 086006 (2009).
[10] H. Liu, J. McGreevy, and D. Vegh, Phys. Rev. D **83**, 065029 (2011).
[11] M. Cubrovic, J. Zaanen, and K. Schalm, Science **325** 439 (2009); arXiv:0904.1993.
[12] T. Faulkner, H. Liu, J. McGreevy, and D. Vegh, Phys. Rev. D **83**, 125002 (2011).
[13] S. A. Hartnoll, Classical Quantum Gravity **26**, 224002 (2009).
[14] J. McGreevy, Adv. High Energy Phys. **2010**, 723105 (2010).
[15] S. A. Hartnoll, arXiv:1106.4324.
[16] S. Sachdev, *Quantum Phase Transitions* (Cambridge University Press, Cambridge, England, 2011), 2nd ed..
[17] T. Mehen, I. W. Stewart, and M. B. Wise, Phys. Lett. B **474**, 145 (2000).
[18] Y. Nishida and D. T. Son, Phys. Rev. D **76**, 086004 (2007).
[19] Y. Nishida and D. T. Son, arXiv:1004.3597.
[20] D. T. Son, Phys. Rev. D **78**, 046003 (2008).
[21] K. Balasubramanian and J. McGreevy, Phys. Rev. Lett. **101**, 061601 (2008).
[22] A. Adams, K. Balasubramanian, and J. McGreevy, J. High Energy Phys. 11 (**2008**) 059.

[23] C. P. Herzog, M. Rangamani, and S. F. Ross, J. High Energy Phys. 11 (**2008**) 080.
[24] J. Maldacena, D. Martelli, and Y. Tachikawa, J. High Energy Phys. 10 (**2008**) 072.
[25] A. Adams, C. M. Brown, O. DeWolfe, and C. Rosen, Phys. Rev. D **80**, 125018 (2009).
[26] E. Imeroni and A. Sinha, J. High Energy Phys. 09 (**2009**) 096.
[27] A. Akhavan, M. Alishahiha, A. Davody, and A. Vahedi, Phys. Rev. D **79**, 086010 (2009).
[28] R. G. Leigh and N. N. Hoang, J. High Energy Phys. 03 (**2010**) 027.
[29] L.-Y. Hung, D. P. Jatkar, and A. Sinha, Classical Quantum Gravity **28**, 015013 (2011).
[30] A. Adams and J. Wang, New J. Phys. **13**, 115008 (2011).
[31] R. Mahajan and J. Wang (unpublished); R. Mahajan, B.S. thesis, MIT, 2011.
[32] N. Iqbal and H. Liu, Fortschr. Phys. **57**, 367 (2009).
[33] T. Senthil, Phys. Rev. B **78**, 035103 (2008).
[34] T. Senthil, Phys. Rev. B **78**, 045109 (2008).
[35] See Supplemental Material at http://link.aps.org/supplemental/10.1103/PhysRevD.89.046008 for the program code.
[36] M. Henneaux, arXiv:hep-th/9902137.
[37] M. Guica, K. Skenderis, M. Taylor, and B. C. van Rees, J. High Energy Phys. 02 (**2011**) 056.
[38] B. C. van Rees, arXiv:1206.6507.
[39] A. Damascelli, Z. Hussain, and Z.-X. Shen, Rev. Mod. Phys. **75**, 473 (2003).
[40] J. I. Kapusta and C. Gale, *Finite-temperature Field Theory, Principles and Applications* (Cambridge University Press, Cambridge, UK, 2006), p. 428.
[41] D. R. Gulotta, C. P. Herzog, and M. Kaminski, J. High Energy Phys. 01 (**2011**) 148.
[42] N. Iqbal, H. Liu, and M. Mezei, arXiv:1110.3814.
[43] C. M. Varma, P. B. Littlewood, S. Schmitt-Rink, E. Abrahams, and A. E. Ruckenstein, Phys. Rev. Lett. **63**, 1996 (1989).
[44] S. Sachdev, Phys. Rev. D **84**, 066009 (2011).
[45] L. Huijse and S. Sachdev, Phys. Rev. D **84**, 026001 (2011).
[46] J. Hartong and B. Rollier, J. High Energy Phys. 01 (**2011**) 084.
[47] S. Cremonesi, D. Melnikov, and Y. Oz, J. High Energy Phys. 04 (**2010**) 048.
[48] S. A. Hartnoll, D. M. Hofman, and D. Vegh, J. High Energy Phys. 08 (**2011**) 096.
[49] C. P. Herzog and J. Ren, J. High Energy Phys. 06 (**2012**) 078.
[50] J. W. Chen, Y. J. Kao, and W. Y. Wen, Phys. Rev. D **82**, 026007 (2010).
[51] T. Faulkner, G. T. Horowitz, J. McGreevy, M. M. Roberts, and D. Vegh, J. High Energy Phys. 03 (**2010**) 121.
[52] P. Kovtun and D. Nickel, Phys. Rev. Lett. **102**, 011602 (2009).
[53] J. Wang (to be published).
[54] K. Balasubramanian and J. McGreevy, J. High Energy Phys. 01 (**2011**) 137.
[55] J. L. F. Barbon and C. A. Fuertes, Phys. Rev. D **80**, 026006 (2009).
[56] S. A. Hartnoll, J. Polchinski, E. Silverstein, and D. Tong, J. High Energy Phys. 04 (**2010**) 120.
[57] S. A. Hartnoll and A. Tavanfar, Phys. Rev. D **83**, 046003 (2011).
[58] S. A. Hartnoll and P. Petrov, Phys. Rev. Lett. **106**, 121601 (2011).
[59] M. Cubrovic, Y. Liu, K. Schalm, Y.-W. Sun, and J. Zaanen, Phys. Rev. D **84**, 086002 (2011).